Engineering a Decorin Surface Coating and Evaluating the
Role of Decorin in the Foreign Body Response to Implants

Marisa L. Sylvester

A dissertation
submitted in partial fulfillment of the
requirements for the degree of

Doctor of Philosophy

University of Washington

2012

Reading Committee:
Buddy D. Ratner, Chair
James D. Bryers
Marta Scatena

Program Authorized to Offer Degree:
Department of Bioengineering

University of Washington

Abstract

Engineering a Decorin Surface Coating and Evaluating the
Role of Decorin in the Foreign Body Response to Implants

Marisa L. Sylvester

Chair of the Supervisory Committee:
Professor Buddy D. Ratner
Department of Bioengineering

Encapsulation of medical devices after implantation leads to reduced functionality and

device failure of long term implants. To improve healing around implants, and allow

long-term implant functionality, the prevention of fibrous encapsulation is necessary.

One of the key players in the development of fibrosis is the pro-fibrotic cytokine

transforming growth factor beta, whose activity can be neutralized by the proteoglycan

decorin, a natural inhibitor of fibrosis. Decorin has demonstrated reduced fibrosis and

improved outcomes in numerous models of fibrotic disease and scar tissue formation

and thus its ability to reduce fibrous encapsulation around an implant was evaluated.

In this work, a novel decorin surface coating was created, characterized, and evaluated

as a method for local delivery of decorin to an implant site. In order to rapidly and

inexpensively screen and optimize novel therapies for fibrous encapsulation, the chick chorioallantoic model was evaluated as an alternative to standard rodent implantation models. This model was less effective and more restrictive than rodent implant models and thus further evaluation of decorin was carried out in rodent models. Fibrous encapsulation and angiogenesis surrounding decorin-coated and uncoated implants were evaluated in a subcutaneous implant model and found to be similar between the two groups. To further evaluate the therapeutic value of decorin against fibrous encapsulation, a cell-based decorin delivery implant model was developed. This model combined porous polymer implants with a smooth muscle cell-based overexpression system to deliver decorin continuously at an implant site. Decorin overexpression demonstrated no differences in capsule thickness, density, angiogenesis or macrophage infiltration at the implant site demonstrating that decorin would not be a promising therapeutic for inhibiting the FBR, though it has been shown to hold promise in other pathological models of fibrosis. This work provides a novel decorin surface coating that holds potential for use in tumor models and further demonstration for the broad applicability of a collagen affinity coating. Further, a model for delivering molecules of interest at an implant site and evaluating effects on the foreign body response was developed in this work. This model provides an effective method for evaluating future therapies for fibrous encapsulation.

Table of Contents

List of Abbreviations…………………………………..……………………… x

Chapter 1: Introduction

1.1   Significance ……………………………………………………… 1

1.2   Foreign body response…………………………………………. 2

1.3   Strategies to reduce fibrous encapsulation…..………………. 3

1.4   TGF-β…………………………………………………………... 5

1.5   Decorin ………………………………………………………… 6

1.6   Decorin TGF-β interactions………………………………….. 8

1.7   Role of decorin in angiogenesis ………………………………. 10

1.8   Collagen affinity coating ……………….……………………. 11

1.9   Experimental models for the foreign body response…………… 12

1.10   Hypothesis and specific aims of thesis……………………….. 13

1.11   Outline of thesis content ……………………………………….. 15

Chapter 2: Design and Characterization of Decorin Surface Coating

2.1   Introduction ………………………………….…………………… 17

2.2   Materials and methods …………………………….…………….. 18

        Creation of model implants……………………….……………… 18

                Casting of bulk pHEMA gels……………………………… 18

                Spincoating of pHEMA ………………………………….. 18

                Preparation of collagen affinity coating………………….. 19

                Verification of decorin binding to collagen in SPR……….. 20

        Attachment of decorin……………………………………….. 20

        Surface characterization…………………………..……………... 21

                TFEA derivatization to confirm CDI activation of surface.. 21

                Verification of surface composition in ESCA ……………..22

List of Figures

List of Abbreviations

ABC	Avidin-biotin enzyme complex
ANOVA	Analysis of variance
ASMC	Aortic smooth muscle cell
bFGF	Basic fibroblast growth factor
BSA	Bovine serum albumin
CAM	Chick chorioallantoic membrane
CDI	1,1' carbonyl diimidazole
CHO	Chinese hamster ovary
COL	Collagen
DAB	3,3'-Diaminobenzidine
DCN	Decorin
DI	Deionized
DMEM	Dulbecco's modified Eagle medium
ECM	Extracellular matrix
EDC	1-ethyl-3-(3-dimethyl aminopropyl) carbodiimide
EGFR	Epidermal growth factor receptor
EMA	Ethyl methacrylate
FBR	Foreign body response
FBS	Fetal bovine serum

GAG	Glycosaminoglycan
H&E	Hematoxylin and eosin
HEMA	Hydroxyethyl methacrylate
HUVEC	Human umbilical vein endothelial cell
LAP	Latency-associated peptides
LRR	Leucine-rich repeats
LTBP	Latent TGF-β binding proteins
MAA	Methacrylic acid
MAP	Mitogen-activated protein
MECA-32	Mouse pan-endothelial cell antigen
MMP	Matrix metalloproteinase
Mv1Lu	Mink lung epithelial cell
NHS	*N*-hydroxysuccinimide
NO	Nitric oxide
PBS	Phosphate buffered saline
PDGF	Platelet derived growth factor
PEO	Poly(ethylene oxide)
pHEMA	Poly-2-hydroxyethyl methacrylate
PMMA	polymethyl methacrylate
SEM	Scanning electron microscopy

SLRP Small leucine rich proteoglycan

SMC Smooth muscle cell

SPR Surface plasmon resonance

TCPS Tissue culture polystyrene

TEGDMA tetraethyleneglycol dimethacrylate

TFEA 2,2,2-Trifluoroethylamine

TGF-β Transforming growth factor beta

ToF-SIMS Time-of-flight secondary ion mass spectrometry

VEGF Vascular endothelial growth factor

Acknowledgements

Chapter 1

Introduction

1.1 Significance

Medical devices comprise a $105.8 billion industry in the United States[1]. These devices cover a broad range of applications from cardiac interventions such as stents and defibrillators to blood glucose sensors[1]. Implantation of these devices into human tissues begins a cascade of events commonly referred to as the foreign body reaction. This cascade of events leads to development of a dense, avascular, collagenous capsule around the implanted device and can result in device failure[2, 3]. The development of biomaterials that promote healing is necessary to combat the current state of inflammation and encapsulation that surround today's medical devices. Especially in the case of implantable sensors, the host response often causes device damage and failure, preventing successful long-term device function[4-6]. The goal of this thesis is to combat fibrous encapsulation by presenting bioactive molecules at the implant site that can promote healing rather than deposition of collagenous scar tissue. It is desirable to achieve local presentation of these bioactive molecules in order to enhance efficacy in reducing fibrous encapsulation at an implant site. Furthermore, local application would avoid undesirable systemic disruption of normal collagenous tissues such as skin, cartilage and tendon[7]. Towards this end, the anti-fibrotic proteoglycan decorin was evaluated as an inhibitor of fibrous encapsulation, both as a bioactive coating and

through local cellular overexpression. With the ability to affect collagen deposition[8-10], blood vessel formation[11-14] and transforming growth factor beta (TGF-β) signaling[15-17], decorin demonstrated the potential to promote healing in a number of animal models[18-27]. Thus, it was expected that application of decorin may lead to long-term functionality of implantable medical devices which have previously suffered from loss of function and failure due to fibrous encapsulation.

1.2 Foreign body response

Implantation of a foreign material into the body, such as a medical device, fosters chronic inflammation and leads to a runaway wound healing process known as the foreign body response (FBR). This process is characterized by rapid protein adsorption to the surface of the implant followed soon after by infiltration of inflammatory cells[28]. Unlike a true healing response to a simple cut, host cells are unable to remove the foreign material from the wound area. As macrophages unsuccessfully attempt to phagocytose and destroy the biomaterial, macrophage fusion and foreign body giant cell formation occurs. Within weeks the implant can be surrounded by a dense, fibrous capsule[28-30]. This primarily avascular capsule can create a significant diffusion barrier even to small molecules, and was demonstrated to be nearly impermeable to a model analyte fluorescein[31, 32]. This capsule provides a challenge for medical devices whose successful function relies on integration with host tissues or communication with the body. In some cases, such as with implantable sensors, the foreign body reaction can

lead to implant malfunction or failure[4, 30, 33, 34]. In the case of implantable glucose sensors, function is lost within days of implantation[5, 6]. Furthermore, in many cases, this dense capsule can contract and lead to performance failures of medical implants such as hernia meshes and mammary prostheses[35-39].

1.3 Strategies to reduce fibrous encapsulation

Research on strategies to reduce foreign body encapsulation have focused on reduction of capsule density, reduction of capsule thickness, or increasing capsule permeability by enhancing vascularization. With the goal of reducing capsule thickness and/or density, much work has gone into creating nonfouling surfaces which reduce initial nonspecific protein adsorption[40-42]. Poly(ethylene oxide) (PEO)[42] and similar tetraglyme[43, 44] coatings have applied to the surfaces of biomaterials and have been shown to reduce protein adsorption[42] although these coatings have not additionally demonstrated reductions in fibrous encapsulation. The most successful report of decreases in fibrous encapsulation involved the development and use of a nitric oxide (NO) releasing polymer coating. The coating demonstrated a reduction of nearly 30% of capsule thickness as compared to control implants although the exact mechanism for the reduction in fibrous encapsulation caused by the NO coating was not elucidated[45].

Attempts to increase capsule vascularity have often focused upon delivery of pro-angiogenic factors such as vascular endothelial growth factor (VEGF)[46-48]. While

effective at increasing neovessel formation, VEGF delivery has been met with the challenges of both short term effects[47], and increases in inflammatory cell recruitment[48]. In order to extend positive effects of VEGF, sustained delivery may be necessary. However, decreasing the corresponding inflammatory cell recruitment has proved to be a more difficult challenge for researchers. Inflammatory cell recruitment was successfully reduced with the addition of dexamethasone, although this also reversed the desired effects on angiogenesis[48]. Increases in vascularity have also been observed through differences in biomaterial surface architecture. Porous implants have been shown to develop capsules similar in thickness to their nonporous counterparts, but with greater vascularity[49]. Much work in our lab has focused on developing sphere-templated porous materials[50-53]. This templating technique allows for precise control of pore diameter, pore interconnect size, and creates regular and uniform pore geometries. This careful control of material geometries allows for the comparison of differences in healing responses between pore sizes. The dissertation research of Andrew Marshall demonstrated an optimal pore size for increased vascularity within porous implants, and found this size to be approximately 35 μm diameter pores[50].

Although much research has gone into the prevention of fibrous encapsulation, an effective solution remains elusive. Researchers have evaluated various alternatives, including: material chemistries, sizes, surface textures, and surface modifications[45, 54-58]. Surface modifications have involved plasma deposition, protein adsorption, and changes in chemical functional groups presented on the surface[42-44, 56, 59]. Knockout

mouse models have been used to quantify the biological molecules responsible for capsule formation[60-62]. The players involved in formation of a fibrous capsule are also involved in formation of healthy skin, cartilage and other normal tissues. Systemic disruption of decorin expression, a regulator of one key inflammatory agonist, TGF-β, resulted in abnormal collagen deposition as well as fragile skin and connective tissue structures[7]. It is therefore necessary to target the FBR locally at the implant site rather than with systemic delivery of treatment.

1.4 TGF-β

TGF-β belongs to a large family of signaling molecules that have roles in cell differentiation, proliferation and production of numerous matrix proteins and proteoglycans including type I collagen and decorin. There are three mammalian isoforms of TGF-β: TGF-β_1, TGF-β_2, and TGF-β_3 which share 60-80% of their sequence homology[63]. All of these TGF-β isoforms are produced as inactive pro-peptides containing N-terminal latency-associated peptides (LAP) complexed with latent TGF-β binding proteins (LTBP). The 25 kD active TGF-β dimer is produced by proteolytic cleavage of the LAP/LTBP regions[64]. There are three known TGF-β receptors: TGF-β type I, type II, and type III receptors. Binding of active TGF-β to its receptors signals the cell through the SMAD family of proteins, and this signaling activity is controlled by MAP kinase signaling pathways[63-68]. All three TGF-β isoforms inhibit the proliferation of most cell types, but stimulate proliferation and matrix

synthesis in mesenchymal cells[64]. Overproduction of TGF-β has been shown to stimulate fibrosis[69-71] and this cytokine has been implicated in pathological processes involving fibrosis[69]. TGF-β_1 is thought to be a key player in the wound healing process after injury based on its rapid induction[72] and ability to recruit inflammatory cells to the wound site which can then secrete more TGF-β[106]. TGF-β also stimulates production and contraction of extracellular matrix by fibroblasts[73]. In a fetal skin wound model, administration of TGF-β induced scar tissue formation and aided wound closure[74]. In this same model, scar tissue size was found to be proportional to the amount of TGF-β applied[75]. Injection of TGF-β subcutaneously in mice resulted in fibrous tissue formation at the injection site[74]. Similarly, TGF-β injection into chambers, which were then implanted subcutaneously in rats, also induced formation of fibrous tissue[74, 76]. Neutralization of this cytokine has been found to significantly reduce fibrosis[68, 77, 78]. In particular, anti-TGF-β_1 antibody reduced fibrosis in a murine model of granulomatous experimental autoimmune thyroiditis[77] and a surgical tissue graft study[78]. This pro-fibrotic cytokine is thus a promising target for inhibition of fibrous encapsulation.

1.5 Decorin

Also known as dermatan sulphate proteoglycan II (DS-PGII)[79], proteodermatan sulphate[80], PG-S2[81] and PG40[82], decorin is the prototypic member of the group of small leucine-rich proteoglycans (SLRP). This group also consists of biglycan,

lumican, and fibromodulin. Proteoglycans in this family are characterized by several leucine-rich repeats (LRR) consisting of roughly 12 amino acids within a core protein of approximately 40 kD[83]. Decorin contains a single glycosaminoglycan (GAG) side chain linked to serine 4 which, depending on the species, is either chondroitin or dermatan sulphate[83]. Decorin is involved in numerous cellular processes including proliferation, migration, and protein synthesis, and is a regulator of collagen fibrillogenesis[8-10]. It is among the numerous molecules that have been shown to interact with type I collagen[84] with an apparent dissociation constant of 10^{-8} M[85]. The binding site for collagen on the decorin molecule is located between LRRs 5-6[86, 87]. Decorin is essential in collagen organization during fibrillogenesis as demonstrated by a decorin knock out mouse with fragile connective tissues and irregular collagen fibril thickness and organization[7]. In healthy connective tissues, decorin is found near the C-terminus of each fibril with the glycosaminoglycan side chain forming a bridge between decorin molecules along adjacent fibrils. Decorin is a potent signaling molecule that can also interact with TGF-β[15], VEGF[88], and thrombospondin-1[89]. Decorin can bind to the epidermal growth factor receptor (EGFR) thus activating receptor phosphorylation and downstream signaling which results in growth suppression of many cell types including fibroblasts and endothelial cells[90]. Decorin has been shown to inhibit fibrosis and scar tissue formation in several animal models based on its ability to bind and inactivate TGF-β[18-20, 91, 92].

1.6 Decorin-TGF-β interactions

The decorin core protein contains at least two binding sites for TGF-β1 with different affinities[93], both contained in the region of leucine-rich repeats[17]. Through evaluation of recombinant peptides from the decorin core protein, a high affinity binding site for TGF-β was determined to be in the Leu155-Val260 peptide sequence whose K_d of 6.8×10^{-9} M was nearly that of the almost full length peptide Asp45-Lys359 $K_d = 1.3 \times 10^{-9}$ M[94]. Several low affinity binding sites may exist in the leucine rich repeat region of the core with binding affinities in the 10^{-8} M range[94]. Leu155-Val260 also includes the location for the collagen binding site in the decorin core protein (amino acids 152-201)[86, 95]. Collagen-bound decorin maintains its ability to interact with TGF-β suggesting that the collagen binding site is independent of the high affinity TGF-β binding site on the decorin core. It has been demonstrated that decorin can form a complex with TGF-β, possibly allowing decorin to regulate TGF-β activity by sequestering it in the extracellular matrix (ECM)[16]. Based on the ability of decorin to interact with TGF-β and collagen simultaneously, the interaction between decorin and TGF-β may be strong enough to keep it from interacting with its receptors that have dissociation constants on the order of 10^{-11} M[94]. TGF-β can be released from this complex by enzymatic degradation of decorin by matrix metalloproteinases (MMPs) 2, 3, and 7. After MMP-mediated release from this complex, TGF-β is not degraded and retains ability to bind to its receptors[16].

Decorin has been shown to neutralize effects of TGF-β in several cellular models[15, 96]. Decorin was able to inhibit the biological activity of TGF-β in Chinese hamster ovary (CHO) cells which overexpress decorin[15]. TGF-β stimulates growth of CHO cells, and addition of decorin to TGF-βstimulated cells reduced the growth below basal levels[15]. Decorin was also able to neutralize TGF-β's stimulatory effects on myofibroblast proliferation[96]. On the other hand, TGF-β inhibits the growth of mink lung epithelial (Mv1Lu) cells. Subsequent addition of 1-100 μg/ml of decorin also reduced the effect of 0.5 ng/ml of TGF-β but did not counteract it completely. The authors suggested that the mechanism of decorin action is binding and neutralizing TGF-β activity[15].

In numerous fibrotic disease models, decorin has been shown to reduce fibrosis and improve outcomes[18-21]. The antifibrotic effects of decorin have been attributed to its ability to bind and inactivate TGF-β[15, 17]. This interaction has been shown to reduce fibrosis in a rat model of kidney fibrosis[19, 21], a hamster model of lung fibrosis[20], and a rat arterial injury model[18]. Intravenous injection of decorin daily for 4-6 days showed significant reduction in matrix accumulation in the kidney disease model while injection of decorin for only two days had little effect. Although decorin accumulates in the kidney, liver and lung, no toxicity was observed during kidney analysis[21]. In the same model, an antibody directed against TGF-β1 was also able to reduce matrix accumulation[97], supporting the idea that decorin activity against TGF-β may provide these beneficial effects. Decorin has an advantage over antibodies of being able to

neutralize all three isoforms of TGF-β, thus having broader applications while each antibody is directed against a single isoform[21]. Decorin has also been shown to reduce smooth muscle cell migration, proliferation, and collagen synthesis in response to platelet derived growth factor (PDGF) stimulation after arterial injury[98]. Decorin injection (50 μg) into a mouse laceration model resulted in reduced fibrosis and improved recovery of muscle function when the injection was given 2 weeks post injury[96, 99]. In an arterial injury model, decorin overexpression demonstrated reduced collagen deposition. Fischer 344 rat SMCs were transduced to overexpress bovine decorin or transduced with vector alone. When injected into aortas after balloon-injury in rats, ECM accumulation was reduced in decorin-overexpressing cell-seeded aortas compared to controls[100]. These studies have provided strong evidence that application of decorin has reduced fibrosis in fibrotic disease models as well as injury models of scar tissue formation.

1.7 Role of decorin in angiogenesis

While decorin is not expressed in quiescent endothelial cells, decorin expression is induced during angiogenesis[11]. This would suggest a role for decorin in modulating angiogenesis, which is supported by studies demonstrating both stimulatory and inhibitory effects of decorin on angiogenesis. Several studies have demonstrated an ability of decorin to serve a pro-angiogenic role. Decorin has been shown both to promote vascular endothelial cell survival by preventing apoptosis, and to enhance tube

formation[12, 13]. Additional support of a pro-angiogenic role for decorin comes from the observation that formation of new blood vessels is delayed in decorin null mice[11]. This reduction in angiogenesis was observed after cauterized corneal injury and was not associated with changes in TGF-β or VEGF expression in the cornea. On the other hand, decorin has also been shown to serve anti-angiogenic roles. Evidence for an inhibitory role in angiogenesis has been demonstrated by decorin suppression of endothelial cell migration and formation of tube-like structures on thrombospondin-1 surfaces[89]. Additionally, purified native bovine and recombinant human decorin were both able to reduce tube formation in VEGF, bFGF and FBS-stimulated human umbilical vein endothelial cells (HUVECs) cultured on Matrigel-coated surfaces. Both stimulatory and inhibitory effects of decorin on endothelial cells have been demonstrated *in vitro*, yet the role of decorin in modulating angiogenesis in wound healing around implants still remains unclear.

1.8 Collagen affinity coating

The natural ability of decorin to bind to collagen provides a possible method of attaching decorin to a surface in a biologically active conformation, specifically via attachment to a collagen surface. Collagen is one of the most prominent proteins in the human body and its diverse functions include providing mechanical integrity and signaling by serving as a depot for cytokines and growth factors. In our lab, a type I collagen affinity coating was developed that has the ability to present the matricellular

protein, osteopontin, on the surface in a biologically active form[101]. Close to 50 additional biological molecules have been identified that also interact with type I collagen[102] and approximately half of these have their specific sites of interaction pinpointed on the collagen fibril. The most active region for sites of interaction on the fibril is the C-terminus half[102]. This type I collagen affinity coating thus holds the potential to attach a variety of molecules to any surface on which it is immobilized. Specifically here the focus is attachment of decorin. By utilizing this collagen affinity coating, biologically active decorin may be presented on the surface of an implant.

1.9 Experimental models for the foreign body response

Simplified *in vitro* models for fibrous encapsulation that occurs as part of the FBR do not currently exist. Thus for evaluation of fibrous encapsulation, an *in vivo* implantation model is commonly used, and these are primarily rodent implant models[54, 55, 58, 59]. As potential therapies for fibrous encapsulation are developed, it would be desirable to have an alternative method to evaluate these therapies more rapidly and at lower cost than that of standard rodent implant models.

The chick chorioallantoic membrane (CAM) model provides a simplified *in vivo* model for fibrous encapsulation that may bridge the gap between cell culture studies that are often not relevant to wound healing *in vivo* and mammalian models which are higher in cost and require more lengthy studies. The inflammatory and angiogenic responses in

the chick CAM have been found to depend on the chemical and physical structure of the implant[103]. The CAM functions as the main respiratory organ for the chick embryo[104]. The CAM lines the inner shell membrane of a fertilized egg, serves in transport of sodium, chloride and calcium into the vasculature, forms part of the allantoic sac wall and collects excreted waste[105]. The normal CAM measures approximately 200 μm in thickness and is composed of the ectoderm layer (multilayered epithelium), stroma and then endoderm (single layer of epithelium) as you move from the shell-side inward. This membrane is used in a well-established angiogenesis model[103, 106] and has been reported to produce a fibrous capsule around implants[105, 107, 108]. Work has been performed with the chick embryo in the shell (*in ova*)[105] or cultured in a Petri dish (*ex ova*)[107, 108]. Development of the chick embryo in the CAM model usually continues for up to 21 days, and is similar for the *in ova* and *ex ova* models[107]. Biomaterials have been implanted into the CAM for up to 11 days and both acute and inflammatory responses have been studied[105, 107]. The CAM model thus presents an attractive technique for use in optimizing implant surface coatings and evaluating the FBR.

1.10 Hypothesis and Specific Aims of Thesis

Hypothesis: Reduced encapsulation and therefore improved healing of implants can be achieved by local presentation of decorin at the implant site.

Specific Aim 1:   Design and characterize a decorin surface coating

Decorin overexpression and injection have been shown to reduce fibrosis in several animal models.   These beneficial effects are attributed to its ability to bind and inactivate the pro-fibrotic cytokine TGF-β. Decorin is therefore a promising molecule to employ as a surface coating to reduce fibrous encapsulation of implants. Decorin was attached to the surface of a polymer implant via a type I collagen affinity coating. This decorin coating was characterized to ensure expected surface composition in ESCA. Decorin attachment to the surface was evaluated in ToF-SIMS, and quantified by radiolabeling. To verify biological activity of this decorin coating, binding of TGF-β to the surfaces was quantified.

Specific Aim 2:   Evaluate healing and encapsulation around decorin implants

To determine efficacy of decorin surface coatings in reducing fibrous encapsulation and improving healing around implants, their functionality must be evaluated *in vivo.* Decorin-coated and control samples were initially assessed in a chick chorioallantoic membrane model as a simplified *in vivo* method of measuring encapsulation. Decorin-coated implants and controls were then evaluated in a mouse subcutaneous implant pilot study. Study results indicated a need for a greater understanding of the role of decorin in healing around implants. Thus decorin overexpression was evaluated to determine the effects a sustained excess of decorin has on fibrous capsule formation and angiogenesis around implants. This aim allowed us to develop an *in vivo* model to

evaluate the effects of decorin overexpression on fibrous encapsulation and angiogenesis as well as evaluate surface attachment of decorin as an effective means of local delivery.

1.11 Outline of Thesis Content

This thesis evaluates the use of the antifibrotic proteoglycan decorin for reduction of fibrous encapsulation around implanted polymeric biomaterials. In this chapter, the biological response to implanted biomaterials was introduced. Specifically the role of transforming growth factor beta (TGF-β) in inducing fibrosis was discussed, and numerous animal models demonstrating the ability of decorin to both inactivate TGF-β and reduce fibrosis were summarized. Current research on fibrous encapsulation therapies was presented, yet there still exists a pressing need for new strategies to address the issue of fibrous encapsulation of implants.

A novel decorin surface coating was created as a means to satisfy this need. The design and characterization of this decorin coating was presented in Chapter 2. A multi-functional collagen affinity coating was employed as a natural means of attaching decorin to the surface of an implant in a biologically active conformation. This coating was thoroughly characterized using a variety of surface analysis techniques to ensure the presence and activity of decorin on the surface.

In Chapter 3 the use of a chick chorioallantoic membrane model was evaluated as a rapid and cost effective assay for assessment of fibrous encapsulation compared to standard rodent models. The ability of this decorin surface coating to reduce fibrous encapsulation was evaluated in a mouse subcutaneous implant model in terms of capsule thickness, density and vascularity.

In Chapter 4, a model was created to evaluate the effects of decorin overexpression on the FBR. This mode of decorin delivery provided increases in both quantity and duration of decorin present at the implant site and allowed measurement of effects on the FBR in terms of capsule thickness, density, angiogenesis and macrophage infiltration.   Finally, in Chapter 5, overall findings from this body of scientific research were summarized and future directions for this work were discussed.

Chapter 2

Design and Characterization of Decorin Surface Coating

2.1 Introduction

Collagen affinity coatings were created on poly(2-hydroxyethyl methacrylate) (pHEMA) model materials and decorin was subsequently allowed to naturally bind to this collagen affinity coating. PHEMA was selected as a base material based on its biocompatibility, ability to resist protein adsorption and cell adhesion, and availability of hydroxyl groups for surface modification[101]. Standard surface characterization techniques were used to verify the successful completion of each step in the coating process, and thus the quality of our final decorin surface coating. Compositions of the pHEMA model surface as well as the 1,1' carbonyl diimidazole (CDI)-activated surface were confirmed using electron spectroscopy for chemical analysis (ESCA). Successful immobilization of collagen to the surface was also verified by ESCA. The quantity of surface-bound as a function of soluble decorin was determined via radiolabeling. The quality of the decorin coating was dependent on its ability to bind TGF-β, which was measured via ELISA.

2.2 Materials and Methods

Creation of Model Implants

Casting of bulk pHEMA gels

Bulk poly-2-hydroxyethyl methacrylate (pHEMA) gels were created by combining 5 ml of 2-hydroxyethyl methacrylate (HEMA) monomer, 0.2 ml of tetraethyleneglycol dimethacrylate (TEGDMA), 1.5 ml of ethylene glycol, 1 ml of water, 0.5 ml of sodium metabisulfite (15% in water) and 0.5 ml of ammonium persulfate (40% in water). The solution was polymerized between 2 glass plates separated by 1mm thick Teflon spacers. The resultant hydrogel was soaked in deionized water to facilitate removal of the glass plates and spacers and remove unreacted monomer. The pHEMA sheet remained in deionized water for several days with fresh water changes each day. Five millimeter diameter disks were cut using a biopsy punch and dried in a vacuum desiccator for 3 days before storing under nitrogen.

Spincoating of pHEMA

Glass disks spincoated with pHEMA were created for use in ultra high vacuum surface analysis techniques including ESCA and time-of-flight secondary ion mass spectrometry (ToF-SIMS). These thin films were created as a substitute for bulk pHEMA gels to facilitate rapid and complete drying of samples, which is necessary for these analysis techniques. Twelve millimeter diameter glass coverslips were coated with a thin layer of pHEMA (Scientific Polymer Products, Inc., Ontario, NY) as

previously described[101]. Disks were cleaned by sonication in methylene chloride followed by acetone and then methanol and allowed to dry. Disks were then coated on both sides by pipetting 10-15 µl of 2.5% (w/v) ethyl methacrylate (EMA)-silane in ethyl acetate onto the surface while spinning at 4000 rpm for 20 s. The coated disks were placed in an oven at 60°C overnight. This was followed by two 1-hour rinses in ethyl acetate with stirring and a subsequent 10 minute methanol rinse. The spincoating procedure was repeated with 15-20 µl of 2.5% (w/v) pHEMA in methanol until all disks were coated on both sides with pHEMA.

Preparation of collagen affinity coating

Dry pHEMA disks underwent three 1,4-dioxane rinses followed by reaction with 20mM 1,1' carbonyl diimidazole (CDI) (Aldrich Chemical Company, Milwaukee, WI) in dioxane for 2.5h at 50°C. The CDI solution was removed and each sample was rinsed three times with dioxane to remove any unreacted CDI. For studies where sterility was necessary, the samples were brought into a chemical laminar flow hood while the third dioxane rinse remained. Dioxane was removed and 300µg/ml collagen (type I rat tail tendon, BD Biosciences) in sodium carbonate-bicarbonate buffer (pH 10.2) was added. The surfaces were allowed to bind overnight at 4°C, followed by three rinses in sodium carbonate-bicarbonate buffer to remove unbound collagen before further use.

Verification of decorin binding to collagen in SPR

Surface plasmon resonance (SPR) was used to verify the ability of bovine decorin (from articular cartilage, Sigma-Aldrich) to bind to rat tail type I collagen. Glass SPR chips (Schott) were coated by gold evaporation (University of Washington Nanotech User Facility). Solutions of 300 μg/ml of collagen, 50 μg/ml of decorin, and 1 mg/ml of bovine serum albumin (BSA, fraction V, Sigma) in PBS (pH 7.4) were prepared and degassed for 30 minutes by sonication under vacuum before use. Deionized water was pumped through the SPR system until stability was reached followed by re-stabilization with PBS. Collagen solution was injected into channel 1 while PBS continued to flow through channel 2 as a control. Collagen was allowed to plateau in adsorption to the gold layer and then followed with PBS injection to wash. The collagen-coated gold surface was then blocked by injection of BSA solution in Channel 1 followed by another PBS wash. Decorin solutions were injected into both channels and allowed to proceed until a plateau was reached followed by a PBS wash. Data were collected by measuring the shift in refractive index seen after each solution change and resultant change in surface-bound protein.

Attachment of decorin

Collagen-coated samples were allowed to naturally bind decorin in solutions of 30, 50, 100 and 150 μg/ml. After incubation overnight at 4°C, samples were rinsed three times

with PBS to remove unbound decorin before use. A schematic of the coating process can be seen in Figure 2.1.
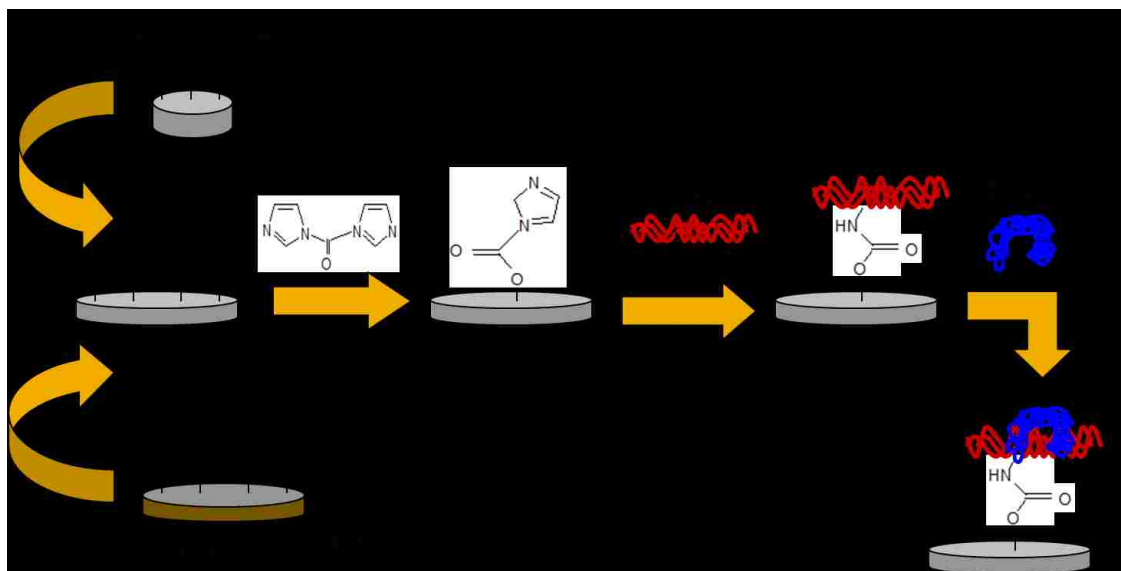
Figure 2.1. Schematic of coating preparation. Hydroxyl groups on pHEMA surface were activated by CDI. Collagen was covalently bound followed by natural attachment of decorin.

Surface Characterization

TFEA derivatization to confirm CDI activation of surface

In order to confirm successful CDI activation of our surfaces, a fluorine derivatization reaction was employed. The fluorinated molecule 2,2,2-trifluoroethylamine (TFEA) (Aldrich) contains a primary amine group which can react with the imidazole carbamate group from CDI. Spincoated pHEMA disks, disks activated with CDI only, and disks activated with CDI plus the collagen affinity coating were reacted with 1.5ml TFEA overnight at room temperature. The samples were placed onto a microscope

slide and the slide was placed in a large glass tube. TFEA was injected into the tube in the space underneath the microscope slide. The tube was backfilled with nitrogen, sealed with a Teflon-coated stopper and left overnight to react. Samples were placed into a desiccator to remove unreacted TFEA and then analyzed by ESCA to determine composition of fluorine on the surface.

Verification of surface composition in ESCA

ESCA was utilized to detect fluorine signals from the TFEA derivatized surfaces as well as verify successful addition of protein to the surfaces. Surface compositions for the top 50-80 angstroms of samples were analyzed on a Surface Science Instruments X-probe ESCA instrument using an aluminum $K_{\alpha1,2}$ monochromatized X-ray source. Spincoated pHEMA samples were analyzed at ultra high vacuum (approximately 10^{-9} torr). An electron flood gun was used to reduce surface charging. A hemispherical energy analyzer set at a 55 degree angle with respect to surface normal was used to measure the energy of emitted electrons. Analysis of spectra was conducted using Surface Science Instruments analysis software with the hydrocarbon peak in the high resolution carbon spectrum set to 285.0 eV as a binding energy reference.

Analysis of protein surfaces in Tof-SIMS

To probe protein-coated surfaces for more detailed molecular information and surface-sensitive composition information, samples were evaluated using time-of-flight secondary ion mass spectrometry (ToF-SIMS). Spincoated pHEMA samples with the

collagen affinity coating as well as the decorin surface coating from the 30 μg/ml solution concentration were evaluated using this technique. As an additional control, a CDI-immobilized decorin coating was created by the same method described previously for CDI-immobilized collagen using a decorin solution concentration of 30 μg/ml.

Positive ion spectra were obtained for static SIMS using a Physical Electronics PHI Model 7200 Reflectron instrument (Eden Prairie, MN) with an 8 keV Cs+ ion source. The primary ion dose was maintained below $1x10^{13}$ ions/cm^2 over an analysis area of 100 x 100 μm. All spectra were calibrated to CH_3+, C_2H_3+, C_3H_5+ and C_7H_7+ peaks with mass calibration errors less than 5 ppm before subsequent analysis. Peaks specific to fragments from any of the 20 amino acids as identified by Lhoest and colleagues[109] were selected for further analysis.

Analysis of SIMS spectra

Selected amino acid peaks were converted into a peak table and then analyzed using the multivariate pattern recognition technique, principal component analysis (PCA). PCA was performed as previously described[110] using standard algorithms implemented with in-house scripts from the National ESCA and Surface Analysis Center for Biomedical Problems (NESAC/BIO) using MatLab (v 5.0, The Math Works, Inc., Natick, MA). Each spectrum was mean centered and normalized to the total intensity of the spectrum before analyzing.

Quantification of decorin by radiolabeling

The amount of decorin on the surface of implants was determined using ^{125}I radiolabeling of decorin. 100μg of decorin was labeled using Iodobeads (Pierce) according to manufacturer's instructions. Two washed and dried beads were added to 0.25ml PBS, with 1mCi of ^{125}I and reacted for 5 min. 100μg of decorin in 0.5ml of PBS was added to the iodine solution and reacted for 15 minutes. Two Biorad Econo-Pac 10 DG chromatography columns were drained and rinsed twice with PBS. The labeled protein solution was added to the first column. PBS was then added to the column in 0.5 ml volumes and fractions were collected. This was repeated until 40 fractions of 0.5ml each were collected for both the labeled protein and unbound iodine. Radioactivity of all 40 fractions was measured by taking 5 μl aliquots and measuring the radioactivity in a Cobra Quantum gamma counter (Packard, model #430660) for 0.1 minute counts. The three fractions containing the labeled protein were added to the second column. Fraction collection was repeated and the three fractions containing the highest radioactivity were retained.

Solutions of 30, 50, 100 and 150 μg/ml of decorin were prepared and spiked with iodinated decorin. Iodinated decorin was counted as 'buffer' for decorin concentration calculations. 5mm diameter bulk pHEMA disks were used for all radiolabeling studies. Bulk pHEMA disks without labeled protein, pHEMA with adsorbed decorin

and pHEMA with adsorbed collagen followed by decorin were prepared in addition to the covalently attached collagen affinity coating with increasing concentrations of decorin in solution. Decorin attachment and collagen affinity coatings were prepared as described previously and activity was measured in the gamma counter from 1 minute counts. Radioactivity was measured on samples in 0.5 ml of PBS in BSA-blocked tubes. After initial counts, sample tubes were incubated at 37 C and the amount of decorin remaining on surfaces over time was measured. At each time point, solutions were removed from tubes, replaced with fresh buffer and activities were measured in the gamma counter.

Quantification of TGF-β binding

The amounts of TGF-β that were able to bind to decorin-coated and control disks were calculated from solution depletion as measured via ELISA. Decorin-coated 5mm diameter bulk pHEMA disks were prepared as described previously (illustrated by the schematic in Figure 2.1) and individual samples were placed in separate wells of a 96-well plate containing 150 μl/well of PBS. A 1 hour incubation of 1 mg/ml of BSA in PBS at 37°C was used to block wells of the 96-well plate before use. Control samples included uncoated pHEMA, CDI + collagen coated pHEMA, and CDI + decorin coated pHEMA (without collagen affinity coating). Decorin-coated samples and control samples were run in triplicate. Recombinant human TGF-β1 (R&D Systems) reconstituted in 4mM HCL containing 1 mg/ml BSA was added to each well to create a final concentration of 2 ng/ml. The plate was incubated at 4°C for 24 hours. A

Quantikine human TGF-β1 solid-phase ELISA (R&D Systems) was used to measure the amount of TGF-β that remained in solution after exposure to samples. The assay was carried out according to manufacturer's instructions. 50 μl aliquots of TGF-β solution from each sample well were added to the pre-coated ELISA plate containing 50 μl per well of Assay Diluent RD1-21. The amount of TGF-β which was bound to each treatment or control disk was calculated by subtracting the measured solution concentration from ELISA and subtracting it from the known quantity of TGF-β which was added to each well. All wells were normalized to the BSA-blocked control well to subtract out nonspecific binding of TGF-β to TCPS plate surfaces.

Blocking of reactive CDI intermediates on surfaces

Binding of TGF-β to CDI + collagen coated surfaces may result from the ability of TGF-β to bind to reactive CDI intermediates that are not bound to collagen fibrils. Since TGF-β has not been shown to interact with type I collagen directly an alternative explanation for the ability to bind in our ELISA should be evaluated. We thus evaluated the ability of lysine and ethanolamine to block all of the reactive CDI intermediates present on the surface. Glass coverslips were spincoated with pHEMA and hydroxyl functional groups on the surface were activated with CDI. Samples were then incubated with sodium carbonate/bicarbonate buffer (pH 10.2), 1M lysine in sodium carbonate/bicarbonate buffer, or 1M ethanolamine in sodium carbonate/bicarbonate buffer overnight at 4°C. Uncoated pHEMA disks served as a negative control. Samples were dried in a stream of nitrogen gas and placed onto a

microscope slide in a large glass tube for a vapor-phase TFEA derivatization reaction. The tube was injected with 1.5ml of TFEA, backfilled with nitrogen, sealed with a Teflon-coated stopper and left overnight to react. Samples were then placed into a desiccator overnight to remove unreacted TFEA and analyzed by ESCA.

2.3 Results and Discussion

Verification of decorin binding to collagen in SPR

SPR was used to verify the ability of bovine decorin to bind to rat tail type I collagen. The refractive index changes associated with the addition of each protein solution followed by PBS rinses are shown in Figure 2.2. The shift in refractive index after each protein addition and PBS wash is proportional to the amount of protein bound to the surface. A large shift in refractive index as demonstrated by collagen binding to gold on Channel 1 indicates a large amount of protein able to bind to the gold surface. The smaller refractive index shift after decorin addition and PBS wash on Channel 1, though less than the amount of decorin which can bind to gold on Channel 2, is confirmation that bovine decorin could bind to the rat tail type I collagen surface.
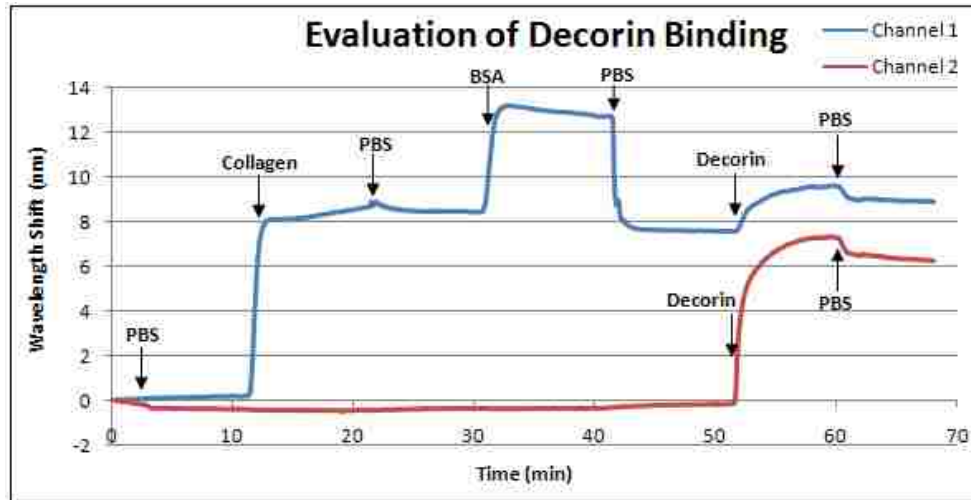
Figure 2.2. SPR evaluation of decorin binding. Plot of refractive index changes associated with addition of collagen (300 μg/ml in PBS), BSA (1 mg/ml in PBS), and decorin (50 μg/ml in PBS) each followed by PBS washes on Channel 1, and decorin (50 μg/ml in PBS) followed by PBS wash on the Channel 2 control.

Surface Characterization

TFEA derivatization to confirm CDI activation of surface

A fluorine derivatization reaction was used to ensure successful activation of pHEMA surfaces. ESCA survey scans showed undetectable levels of fluorine on unmodified pHEMA surfaces, 8.6% fluorine composition on CDI-activated surfaces and 2.8% fluorine on collagen affinity coatings. High resolution carbon scans (Figure 2.3) demonstrate the appearance of a peak consistent with C-F$_3$ at a shift of 7.74 eV from the hydrocarbon peak on the CDI-activated surface. The intensity of this C-F$_3$ peak is reduced on the collagen affinity coating surface.
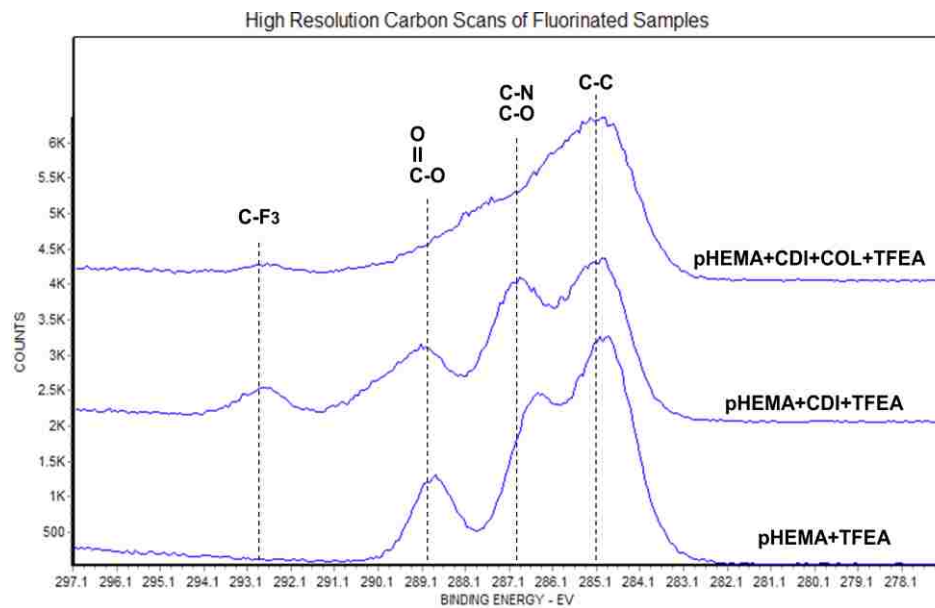
Figure 2.3. ESCA high resolution C1s scans of TFEA derivatized surfaces. The pHEMA surface contains no C-F$_3$ peak (bottom), while the CDI activated surface (middle) demonstrates the appearance of a C-F$_3$ peak at a shift of 7.7 eV from the C-H peak at 285.0. A reduced C-F$_3$ peak is present on the TFEA reacted CDI + collagen surface (top).

Theoretical fluorine composition is 17.6% for a 1 to 1 activation of every hydroxyl group on the surface and 100% binding of TFEA. Assuming steric hindrance of CDI in binding to free hydroxyl groups is the cause of lower actual fluorine composition, we can estimate that approximately 50% of the available hydroxyl groups are activated by CDI. After reaction with collagen, CDI reactive intermediates are still present on the surface as indicated by a 2.8% fluorine signal on collagen-coated surfaces.

Verification of surface composition in ESCA

ESCA was used to characterize the composition of CDI-activated and protein-coated surfaces. Survey scans provided a carbon/oxygen ratio of 67.3/32.7 for spincoated

pHEMA surfaces which is similar to theoretical values of 66.7/33.3. CDI-activation of the surface introduces a nitrogen peak to the composition scan. For 1 to 1 binding of CDI to free hydroxyl groups on pHEMA, a theoretical %N of 12.5 would be obtained. Calculations based on the measured nitrogen signal of 5.7% indicate an activation of 45.6% of available hydroxyl groups. This is in agreement with the CDI/OH ratio obtained from fluorine derivatization. An increase in nitrogen composition to 10.1% indicated the addition of collagen to the CDI-activated surface. The subsequent addition of decorin resulted in similar levels of nitrogen to the collagen surface, which agrees with expectations. Decorin is a proteoglycan, and thus it contributes a nitrogen-rich protein core as well as a carbon and oxygen-rich glycosaminoglycan side chain. Survey scans from CDI-activated spectra are provided in Figure 2.4.
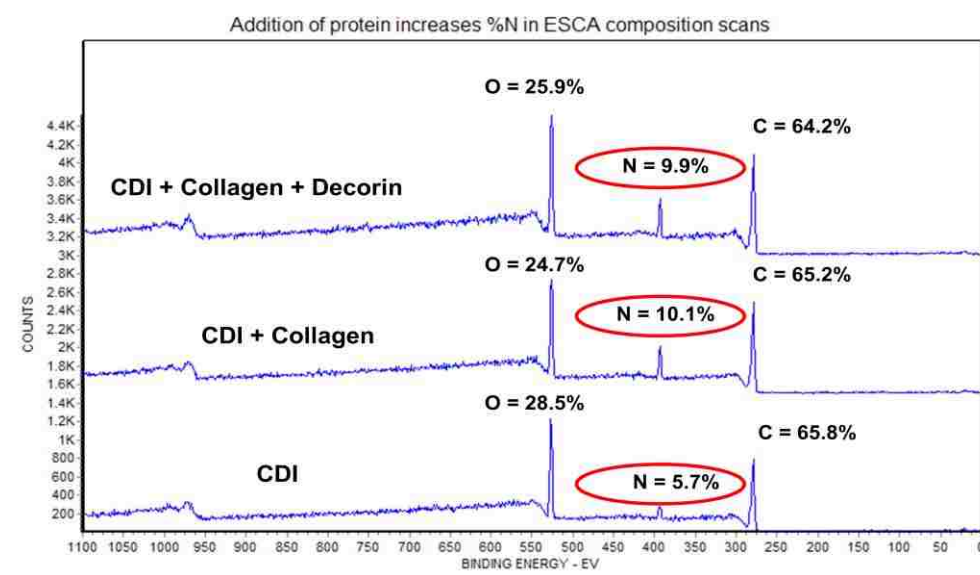
Figure 2.4: ESCA composition scans of coated pHEMA surfaces. Increase in percent nitrogen from CDI-activated pHEMA surface (bottom scan) compared to collagen-immobilized surface (middle scan) and collagen immobilized surface with bound decorin (top scan) indicates successful protein attachment.

<u>Analysis of protein surfaces in Tof-SIMS via PCA</u>

Analysis of SIMS data was focused on elucidating differences in protein structures and compositions between CDI-immobilized decorin (DCN), CDI-immobilized collagen (COL) and CDI-immobilized collagen + decorin (COL+DCN) surfaces. Peaks specific to amino acids were selected and used to determine differences between these protein-coated surfaces through PCA. The first two principal components (PCs) in the model captured 98% of the variance associated with peak intensity differences between surfaces (using the selected peak set). The plot of PC1 vs. PC2 in Figure 2.5 shows distinct clustering of the three separate surfaces. In this model, PC1 can be used to identify differences between the two protein controls and the decorin affinity coating while PC2 can be used to identify differences between collagen and decorin. The loadings plot of PC2 (Figure 2.6) provides information on which amino acids primarily contribute to the separation seen between the decorin and collagen controls. The most pronounced differences can be attributed to a strong proline peak (m/z=70) in COL samples whereas DCN samples contain strong leucine (m/z=86) and lysine (m/z=84) peaks. The large proline content of collagen and the characteristic leucine rich repeats in the structure of decorin lend support to these findings in SIMS spectra. The separation of COL+DCN from DCN surfaces indicates that we are likely seeing both proteins on our coating surface and we do not have complete coverage of collagen by decorin.
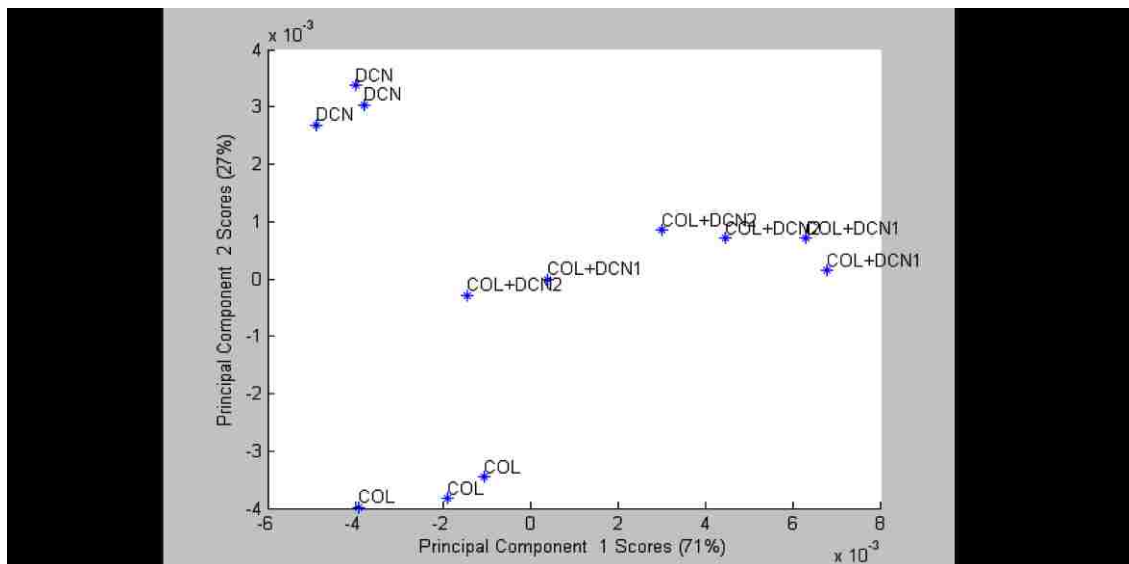
Figure 2.5. PCA Analysis of ToF-SIMS data from coated surfaces. Plot of principal component 1 (PC1)vs. principal component 2 (PC2) shows separation of decorin (DCN), collagen (COL) and collagen + decorin (COL+DCN) surfaces.
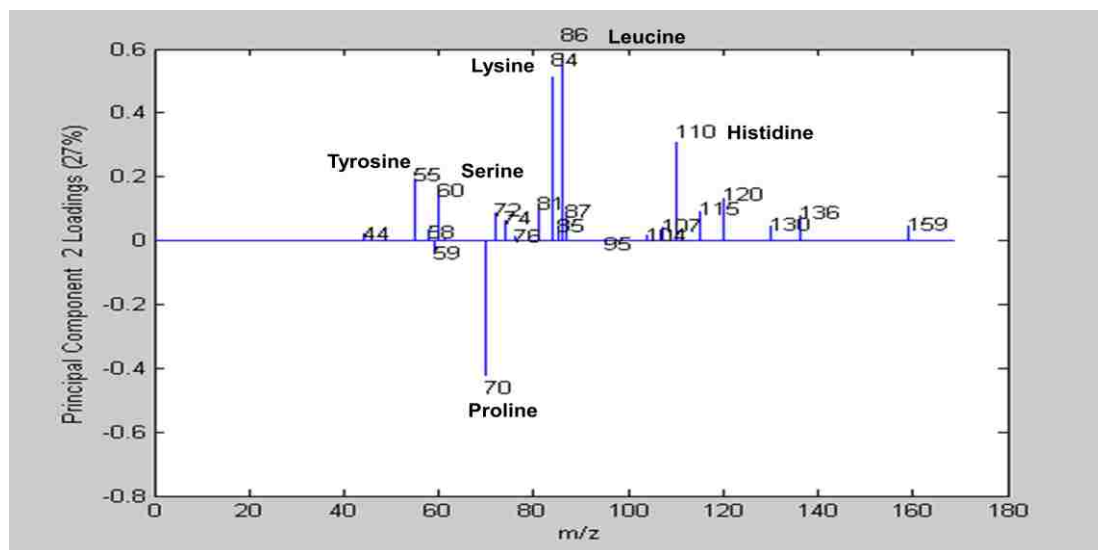
Figure 2.6: PCA loadings plot of principal component 2. Plot demonstrates specific amino acid peaks which are contributing to separation of decorin and collagen surfaces. Decorin samples contain strong peaks corresponding to leucine and lysine while collagen samples contain a strong peak corresponding to proline.

<u>Quantification of decorin by radiolabeling</u>

The amount of decorin able to bind to the collagen affinity coating was measured via radioiodination of decorin. Decorin solution concentrations ranged from 30 μg/ml to 150 μg/ml. Binding of decorin to collagen surfaces was found to be dose-dependent. At the highest solution concentration evaluated, 150 μg/ml, the quantity of decorin bound to the surface was 300 ng/cm^2, which was consistent with a monolayer of decorin at the surface (Figure 2.7). Radiolabeling studies confirmed successful binding of decorin to collagen affinity coatings in quantities which are reasonable for a monolayer of protein. The amounts of decorin which remained on surfaces over time at 37°C are given in Figure 2.8. The majority of decorin was released into solution in the first 24 hours of incubation.
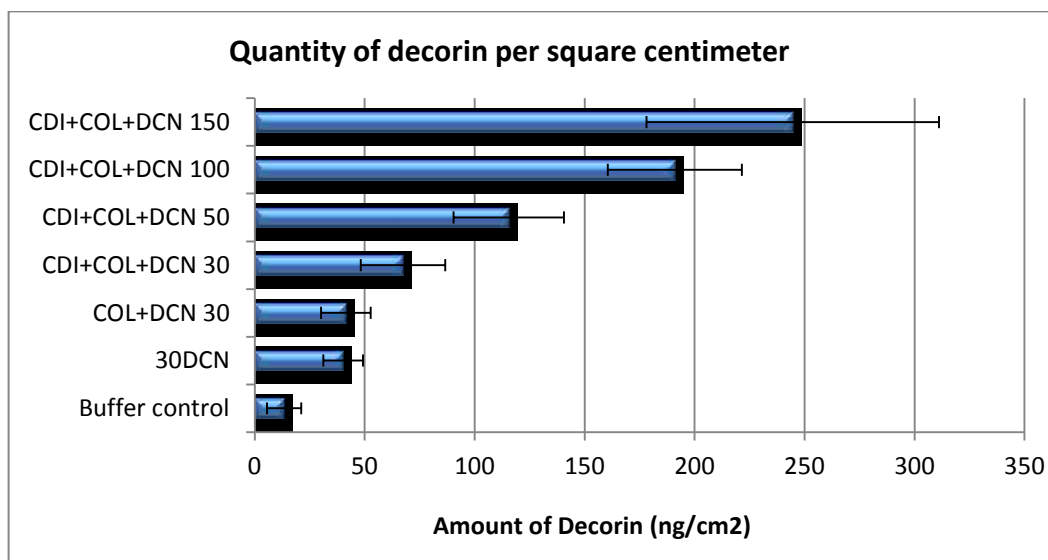
Figure 2.7. Quantity of decorin present on coated surfaces. Samples were incubated with decorin solutions spiked with ^{125}I labeled decorin, washed three times and measurements were taken on a gamma counter. Treatments include pHEMA disks with no protein (buffer), adsorbed decorin (30DCN), adsorbed collagen and decorin (COL+DCN 30) and CDI-activated pHEMA with immobilized collagen with increasing concentrations of decorin listed in μg/ml (CDI+COL+DCN).
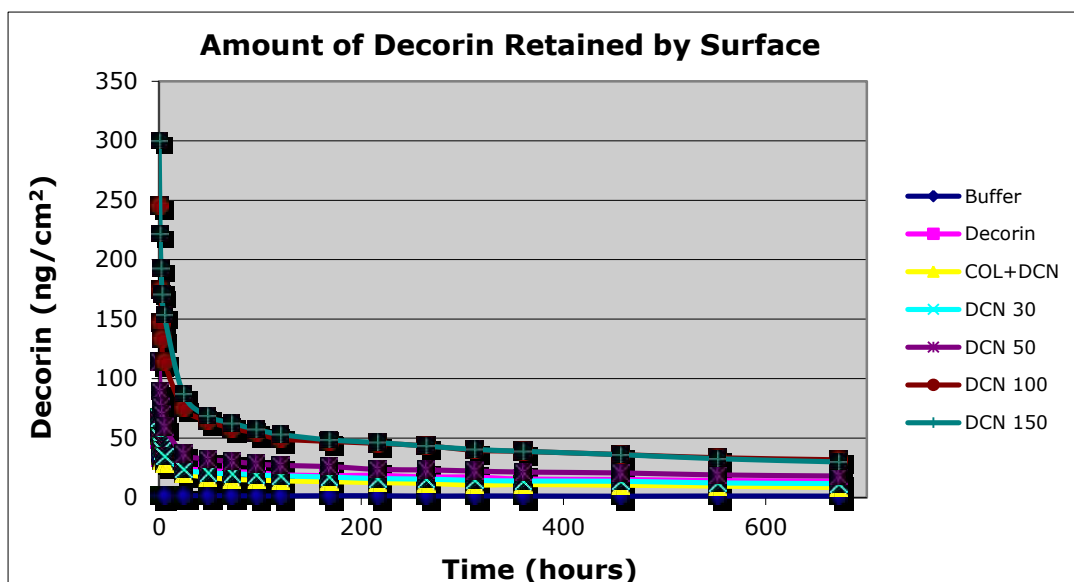
Figure 2.8. Quantity of decorin retained on surfaces over time at 37°C. Samples were incubated with decorin solutions spiked with ^{125}I labeled decorin, washed three times and initial measurements were taken on a gamma counter. Samples were stored at 4°C and were placed in fresh buffer daily to measure radioactivity that remained on sample surfaces over time as a measure of decorin quantity. Treatments include pHEMA disks with no protein (buffer), adsorbed decorin (30DCN), adsorbed collagen and decorin (COL+DCN) and pHEMA with CDI-immobilized collagen and increasing concentrations of decorin in μg/ml (DCN 30, DCN 50, DCN 100, DCN 150).

Quantification of TGF-β binding

The amount of TGF-β which remained in solution after incubation with coated surfaces was measured via ELISA. The highest TGF-β solution concentrations correspond to the lowest amount of TGF-β bound by sample surfaces. PHEMA surfaces bound the lowest amount of TGF-β followed by the BSA-blocked control wells. Although we would have expected control wells to exhibit the least binding, this difference was likely due to nonspecific binding of TGF-β to the surfaces of TCPS wells despite BSA blocking. Surfaces treated with CDI followed by decorin at 30 and 100 μg/ml, bound

the most TGF-β which was similar to that bound by surfaces treated with CDI followed by collagen. High binding by collagen surfaces was not expected as type I collagen is not known to interact with TGF-β. One possible explanation for this finding would be direct binding of TGF-β to reactive CDI intermediates on the surface. Another possibility could be contamination of collagen with decorin that was associated with the fibrils before extraction and which were not removed during purification. Surfaces treated with CDI followed by collagen and then decorin in concentrations of 30, 100 and 150 μg/ml bound slightly less TGF-β than decorin or collagen surfaces alone. A dose response in TGF-β binding when increasing amounts of decorin were bound to the surface was not seen. The amounts of TGF-β remaining after incubation with each sample are given in Figure 2.9 in units of pg/ml. Triplicate samples were run and error bars represent +/- 1 standard deviation from the mean. Measuring exact TGF-β binding by incubating TGF-β solutions with coated surfaces is made difficult by the tendency for TGF-β to bind nonspecifically to many surfaces including TCPS. Although blocked with BSA, these surfaces could still allow TGF-β to bind and affect the accuracy of our results. However, in setting up the experiment, blocked control wells were included to be able to subtract this nonspecific binding from our results.
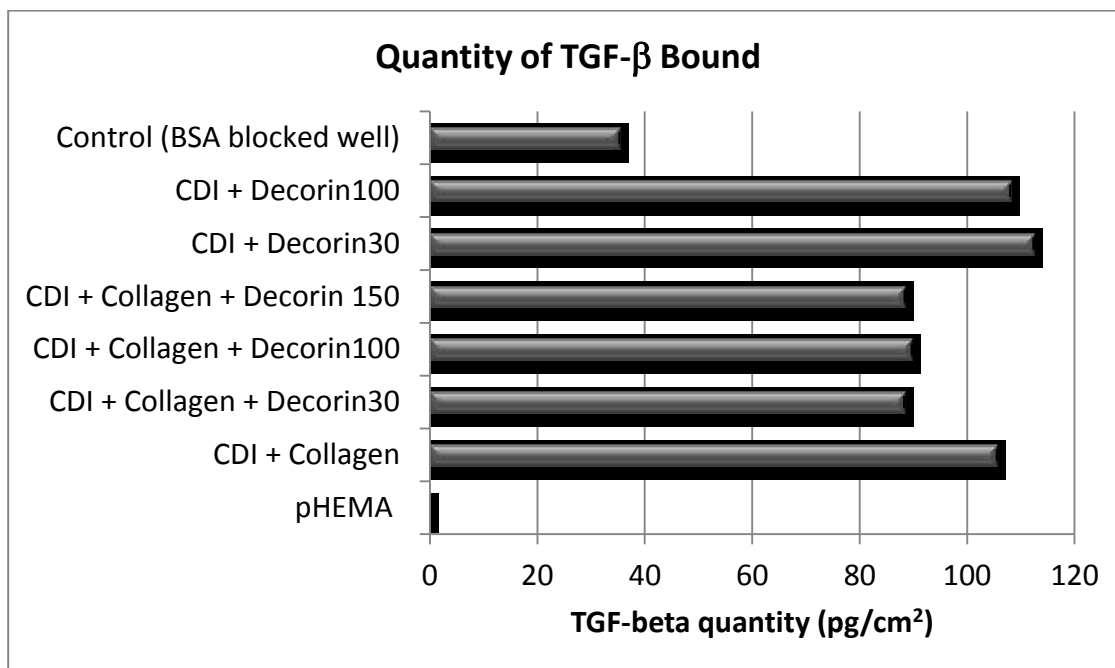
Figure 2.9: Quantity of TGF-β bound to surfaces after sample incubation. Samples included BSA-blocked control well, pHEMA control, and CDI-activated pHEMA with 300 μg/ml solution concentration followed by decorin at 30, 100, or 150 μg/ml or decorin without collagen.

Blocking of reactive CDI intermediates on surfaces

Fluorine derivatization reactions confirmed the presence of reactive CDI intermediates on the surface both after collagen immobilization and after incubation of two separate small molecules for blocking. In the first study, it was shown that collagen blocked approximately 67% of the available binding sites of CDI on the pHEMA surface as indicated by the percentage of fluorine detected in ESCA. In the subsequent blocking study, lysine was able to bind approximately half of the binding sites while ethanolamine was only able to bind one quarter of the sites, both indicated by percentage of fluorine on the surfaces before and after blocking. Though both ethanolamine and lysine were selected due to their small size and presence of a free

amine capable of reacting with CDI, neither molecule was able to completely block available reactive sites. It is expected, then, that some amount of TGF-β binding to the CDI-activated pHEMA surface would be possible and may have had some effect on ELISA binding results.

2.4 Conclusions

This work demonstrated the successful binding of decorin to the surface of a model pHEMA implant via a type I collagen affinity coating. Each step of the coating process was characterized and verified including CDI activation of hydroxyl groups on the pHEMA surface, covalent immobilization of type I collagen and natural binding of decorin. Fluorine derivatization demonstrated an activation efficiency of approximately 50% of surface hydroxyl groups by CDI. The quantity of decorin on the surface was approximately 300 ng/cm^2 based on radiolabeling studies which was consistent with a monolayer of the proteoglycan. It was previously found that decorin binds poorly to denatured collagen[85], thus it can be inferred from the successful binding of decorin that the covalently linked collagen was in a native rather than denatured conformation. Unexpectedly, TGF-β was able to bind to collagen in similar quantities as it was able to bind to decorin coatings. Since TGF-β is not known to have collagen binding ability, we expect that it is binding to reactive CDI intermediates that were not attached to collagen fibrils or that the collagen coating has some decorin contamination that was not removed during extraction and purification in the

commercially available collagen we were using. To evaluate the ability of small molecules to block available CDI reactive intermediates, we tested both ethanolamine and lysine as examples. We found a 50% reduction in fluorine signal when CDI surfaces were blocked with lysine and reduced efficacy with ethanolamine. It was found that neither of these small molecules would be suitable for complete blocking of CDI intermediates.

Chapter 3

Evaluation of Decorin Coating *In Vivo*

3.1 Introduction

Novel decorin surface coatings were successfully created and thoroughly characterized in Chapter 2 of this thesis, and were designed to inhibit or reduce fibrous capsule formation around medical implants. Methods for evaluating therapies to reduce fibrous capsule thickness currently lack a rapid and low cost model. *In vitro* models are unable to accurately reproduce fibrous encapsulation and *in vivo* models are lengthy and costly.

Recently, the chick chorioallantoic membrane (CAM) model has received significant attention as a method for evaluating both fibrous encapsulation of implants [105, 107, 108, 111] and angiogenic responses to treatments[103, 106]. Work has been performed with the chick embryo remaining within the shell (*in ova*)[105] or following removal from the shell and cultured in a Petri dish (*ex ova*)[107, 108, 111]. It was previously found that the *in ova* model is limited by inflammation caused by eggshell dust from windowing, limited access and small sample numbers due to small window area[107]. For ease of implantation and visualization, the *ex ova* model was initially chosen for this work.

The CAM model was evaluated as a simplified *in vivo* model for fibrous encapsulation. This method may bridge the gap between cell culture studies which are often not relevant to *in vivo* wound healing and mammalian models which are expensive and time consuming. The CAM model has the benefits of being inexpensive, easy to handle, and requires a shorter implantation time while providing a foreign body response to implants. Biomaterials have been implanted into this membrane for time periods up to 11 days and both acute and inflammatory responses have been studied[105, 107]. The inflammatory and angiogenic responses in the chick CAM have been found to depend on the chemical and physical structure of the implant[103]. For the reasons listed above, the CAM model presented a promising technique to use for optimizing various surface coatings for implants and evaluating healing responses.

Further analysis of the decorin surface coating was carried out in a mouse subcutaneous implant model. Coated surfaces whose creation and characterization was laid out in Chapter 2 of this thesis were evaluated for ability to promote healing around implants. Decorin-coated implants and uncoated pHEMA control implants were evaluated after a 28 day implantation for effects on fibrous capsule thickness, density and angiogenesis.

3.2 Materials and Methods

CAM Assay

Ex ova CAM assay

Evaluation of healing response to coated and uncoated pHEMA implants were carried out in the CAM model as published with modifications[107]. Fertilized chicken eggs (Hyline Farms, Puyallup, WA) were placed horizontally in an egg incubator for 3.5 days at 37º C. While disturbing the contents of the egg as little as possible, the eggs were cleaned with 70% ethanol, cracked on the bottom surface and placed in pre-warmed, sterile, polystyrene Petri dishes and covered. Dishes were carefully placed in another 37º C egg incubator. At day 7 of incubation, coated and uncoated bulk pHEMA disks (5mm diameter, 1mm thick) were implanted into each CAM by gently placing each implant on top of the CAM approximately ½ cm from the embryo.

Optimization of implant samples and procedures

Samples for implant were optimized both to improve embryo survival, and to enhance visualization for explantation procedures. Initial 5 mm diameter pHEMA implants were reduced in size to 1 mm diameter. Challenges with finding these small transparent implants in the CAM led to use of numerous histological dyes and food coloring to aid in visualization of the polymer implants. An opaque material was finally selected for ease of locating samples for explants. Braided silk sutures were selected for roughness to aid in incorporation as well as ability to dip coat in pHEMA

for attachment of surface coating. Silk sutures were dip-coated with pHEMA (5% w/v, Scientific Polymer Products, Inc., Ontario, NY) in methanol, and each suture received three coats of pHEMA to ensure complete coverage. Implant samples were either pHEMA dip coated control samples, or pHEMA dip coated and further decorin-coated samples. Samples to be decorin coated were CDI activated, collagen was covalently attached and decorin was allowed to bind to collagen (as described in Chapter 2 for pHEMA disks). To further improve embryo survival, implantation procedures were moved to the *in ova* model rather than the *ex ova* model that was initially selected. Cutting a small window in the top of each shell was presumed to disturb the developing embryo less than complete removal from the shell.

In ova CAM assay

Evaluation of healing response to pHEMA control and decorin-coated implants were carried out in the CAM model as published with modifications[105]. Fertilized chicken eggs (Hyline Farms, Puyallup, WA) were placed horizontally in an egg incubator and turned twice daily for 3 days at 37 C. On day 4, each egg was cleaned with 70% ethanol, and a 1 cm x 1 cm window was cut into the shell, and clear plastic was taped in place to prevent contamination and allow visualization. At day 7 of incubation, coated silk sutures were gently placed on top of the CAM approximately 0.5 cm from the embryo. Decorin-coated sutures as well as pHEMA and collagen-coated controls were implanted. Samples were allowed to incorporate for 11 days post-implant and then fixed *in situ* with 10% neutral buffered formalin. Samples were then removed

along with the surrounding tissues, paraffin embedded, cut into 5 μm thick sections, and stained with Masson's Trichrome according to manufacturer's instructions. Images were obtained at 4x and 10x on a Nikon E800 upright microscope.

Mouse subcutaneous implant model

Preparation of implant samples

Decorin coating processes were carried out as described in Chapter 2. Briefly, PHEMA gels were created by combining 5 ml of HEMA monomer, 0.2 ml of TEGDMA, 1.5 ml of ethylene glycol, 1 ml of water, 0.5 ml of sodium metabisulfite (15% in water) and 0.5 ml of ammonium persulfate (40% in water). The solution was polymerized between 2 glass plates, soaked in water, cut into 5 mm disks using a biopsy punch. In order to keep pilot study animal numbers at a minimum, disks prepared for implant were either pHEMA control disks or decorin coated disks as illustrated in Figure 3.1. Disks which received the decorin coating for implant were dried, and modified with CDI to covalently link collagen followed by incubation with decorin.
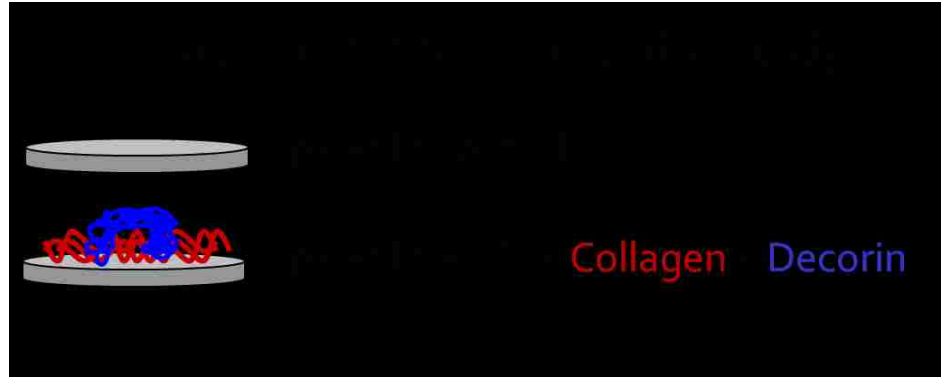
Figure 3.1. Illustrated implants for decorin coating study. All implants were 5 mm diameter pHEMA disks. Treatment includes addition of CDI followed by covalent attachment of collagen followed by decorin binding.

Cytotoxicity and endotoxin assessment

The fibroblast cell line, NIH 3T3, was used according to ISO standard 10993-5 to evaluate cytotoxicity of implant materials made in the same batch as were implanted. Cells were seeded in 12-well TCPS plates in one ml of growth media (High glucose DMEM with 10% FBS, 1% l-glutamine, and 1% sodium pyruvate) per well. Samples were incubated for 24 hours in growth media at a volume of 3 ml media per 9 cm^2 of surface area. Latex punched from pipette bulbs with a 5 mm diameter biopsy punch was sterilized in 70% ETOH for 8 hours, rinsed in 40 ml DI water with 4 water changes after 15 minutes each, and then soaked in growth media overnight as a positive control. Media incubated in TCPS wells served as a negative control. Cells were cultured for one day in growth media and then the media was aspirated off, media from TCPS, decorin coated samples or negative control wells were then added to cell wells, and cells were cultured for an additional 48 hours. Cells were visualized under a microscope at 24 and 48 hours for signs of toxicity. Threshold endotoxin testing was

carried out using Cambrex Bioscience Limulus Amebocyte Lysate Pyrogent Plus kit according to manufacturer's instructions.

Subcutaneous implantation

Three male 7wk old C57BL6 mice weighing approximately 20 g each were used for implantation. The implantation protocol was approved by the University of Washington IACUC (Institutional Animal Care and Use Committee). Each mouse received an IP injection of 0.4ml of anesthesia cocktail (0.16 ml Ketamine and 0.055 ml Xylazine diluted in 2.28 ml saline). Each mouse received a dot of eye gel in each eye to prevent drying, was shaved from just below the shoulders to just above the tail, and rubbed with Betadine to prepare the skin for surgery. An ethanol rub was used to remove the Betadine from the skin. Surgeries were performed on clean pads placed on a water circulating warming pad set to 37°C to prevent heat loss from mice. Each mouse was placed in the prone position and a dorsal incision was made with a sterile scalpel just offset from the spine about 2cm in length. Care was taken to cut just through the skin and not into the underlying muscle. Blunt dissection scissors were used to create 4 separate subcutaneous pockets, one behind the forelimbs on each side and one in front of the hind limbs on each side of the mouse. Both anterior and posterior implant locations received an uncoated pHEMA implant and a decorin-coated pHEMA implant. Placement of coated and uncoated implant on right or left side of each location was randomized in this study by blocking for anterior and posterior locations and randomizing within locations. After creation of each subcutaneous

pocket, the appropriate implant was removed from the sterile 12- well plate where it was immersed in either PBS for uncoated implants or 150 µg/ml of decorin in PBS for coated implants. Implants were placed deep into pockets to try to prevent migration toward the incision location during healing. After surgery mice received 0.1 ml of Buprenorphine solution (0.01 ml Buprenorphine in 0.3 ml saline) for a dose of 0.05mg/kg of body weight, injected subcutaneously near the base of the tail or on the ventral side near the gut. Mice received standard rodent chow and water during the course of the 28 day study.

Sample explantation and tissue processing

After 28 days, animals were sacrificed and implants and surrounding tissues were removed. Tissue samples were fixed in modified Methyl Carnoy's fixative (90% methanol and 10% acetic acid), paraffin embedded and cut into 5 µm sections for histological analysis.

Measurement of fibrous encapsulation

Tissue sections were stained with Masson's Trichrome according to manufacturer's instructions. Each section had 3 images captured at low magnification (4x). Images were calibrated using a micrometer and capsule thicknesses were measured in Metamorph software at 5 random locations per image. Average thicknesses per section were calculated and compared using t-tests. Where more than two treatments are being

compared, statistical significance was determined with ANOVA with $p < 0.05$ being significant.

Assessment of angiogenesis

Detection of endothelial cells was performed by immunohistochemistry for MECA-32 (BD Biosciences). Paraffin embedded 5 μm sections were baked onto slides, deparaffinized in xylenes and rehydrated to PBS. Sections were peroxidase quenched with 3% hydrogen peroxide in methanol for 30 minutes during rehydration steps. Sections were then incubated with blocking buffer (4% normal goat serum in PBS) for one hour at room temperature, followed by incubation with MECA-32 (diluted 1:10 in blocking buffer) overnight at 4° C. Sections were washed with PBS and incubated with biotinylated goat anti-rat secondary antibody (BD Biosciences) for 1 hour at room temperature followed by a streptavidin-peroxidase complex (ABC) according to manufacturer's instructions. Sections were developed using SigmaFAST DAB, counterstained with hematoxylin, dehydrated and coverslipped with Permount. Any positively stained areas on tissue sections were imaged at 20x to evaluate presence of lumen structures within capsules as a measure of angiogenesis.

3.3 Results and Discussion

CAM Assay

Ex Ova CAM assay

Bulk pHEMA 5mm disks were initially implanted into the CAM model and resulted in high mortality rates. Reduction of implant size to 1 mm diameter disks improved embryo survival but were difficult to locate once placed on the CAM. Development of the chick embryo in the CAM model continues for up to 21 days, just before the chick would hatch, and is similar for both the *in ova* and *ex ova* models[107]. For the *ex ova* model, by day 6 of incubation, the CAM is spread across both the yolk and egg white and development of the vasculature is apparent. The CAM and associated vasculature spread to the edges of the Petri dish by day 13. Due to the reduction of yolk, areas of the CAM begin to appear translucent around day 17[107]. This translucent appearance and the clear nature of pHEMA implants made implants virtually invisible within the CAM.

Optimization of implant samples and procedures

Once pHEMA disk size was reduced, disks could not be found for explant. Numerous histological dyes as well as food coloring were used to aid in visualization of the polymer implants, however, at the end of the study, all disks were clear and undetectable in the surrounding tissue. It was presumed that during CAM development dyes leached from the hydrogel implants. Due to these challenges, an alternate base

material was needed that could be treated with decorin surface coatings, satisfy size limitations, and be visible in the CAM. Woven silk sutures were chosen as replacement base materials because they were opaque and easy to visualize within the CAM, were very small in diameter and could be cut to any length. Sutures were dip-coated with pHEMA and surface modified to attach the decorin coating. Both decorin-coated sutures and pHEMA-coated control sutures were placed onto CAM membranes for evaluation. Through final selection and coating of silk sutures, successful implant optimization was accomplished. However, embryo survival to 11 days post implant, or gestation day 18, remained a challenge. To improve embryo survival further, implants were conducted in the *in ova* model which was presumed to disturb developing embryos far less than complete removal from shells.

In Ova CAM assay

Implantation of coated silk sutures into the *in ova* CAM assay resulted in improved embryo survival and the ability of implants to remain in eggs for the full 11 day study. Histological analysis of CAM explants showed that the majority of samples did not fully incorporate into the membrane as seen in Figure 3.2. Only 1 of 27 successful explanted samples fully incorporated into the CAM. This made it impossible to measure encapsulation of samples and we were unable to make comparisons between groups. A significant amount of effort went into addressing technical challenges in this assay. Samples sizes were reduced to improve embryo survival, sample materials were modified to be more clearly visible and prevent sample loss during explanting, and

histological challenges which were not discussed in this chapter were overcome to enable processing and sectioning of a delicate membrane such as the CAM. Despite these successes, lack of implant incorporation did not allow comparisons of fibrous encapsulation between groups. Similar difficulties with incorporation of implants have been reported[105].
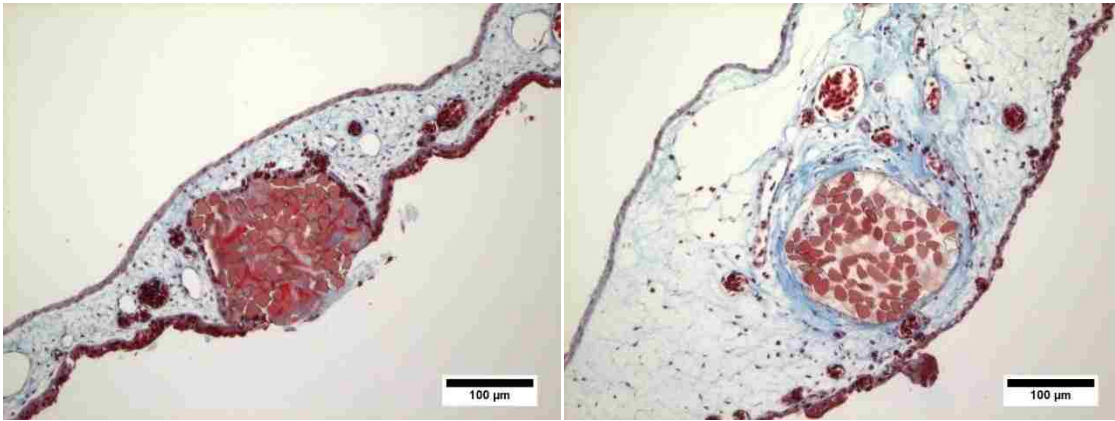
Figure 3.2. Coated silk sutures after 11 day implantation in CAM. Representative images of lack of incorporation of the majority of implanted samples (left). Image of sample that was able to incorporate (right).

The CAM assay has been reported to produce a foreign body response similar to that of rodent models and thus provided a promising assay to evaluate coated samples more rapidly and at reduced cost compared to rodent models. Valdes and colleagues [105] evaluated the CAM response to bacterial endotoxin, cotton thread and silastic tubing placed onto the top of the CAM *in ova*. The silastic tubing, greater in diameter (.064cm OD) and less porous than the thread, did not incorporate fully into the CAM and the membrane grew to half the height of the tubing[105]. The sutures used in this

study were similar in diameter to the cotton thread and significantly smaller in than the silastic tubing and therefore were not expected to pose challenges with incorporation. The authors found difficulty with incorporation of materials that are smooth and do not readily promote cell attachment. Acetaminophen sensors were coated with egg white from the fertilized egg or purchased ovalbumin to aid incorporation in a subsequent study[108]. We found similar challenges with incorporation as described in these studies. Even our protein-coated samples of small diameter met with significant incorporation challenges. In agreement with published reports, we found that the CAM does produce a foreign body reaction. However, the strict limitations on implant size to maintain embryo survival and challenges with incorporation far outweigh the benefits of reduced cost and healing time which initially merited exploration of this assay.

Subcutaneous mouse implant study

Cytotoxicity and endotoxin assessment

Materials to be used for implantation were evaluated for cellular toxicity and endotoxin. Samples for implant, TCPS negative controls and latex positive controls were incubated with media for 24 hours and then this media was transferred to NIH 3T3 cell cultures. After 24 hours, positive control wells contained primarily rounded cells and evident toxicity. Both negative control wells and sample wells had spread cells, which had increased in number and showed no signs of toxicity. At 48 hours, positive control cells showed no growth, few cells remaining on the surface and those

that remained were balled up. Both negative control wells and decorin sample wells had confluent cell populations and demonstrated no visible toxic effects. All samples for implant also tested below detectable levels for endotoxin.

Measurement of fibrous encapsulation

Sections from coated and uncoated implants were stained with Masson's Trichrome and images of capsules were obtained. Capsule thicknesses were measured and compared between groups. Representative images of Masson's trichrome stained sections are given in Figure 3.3 with an uncoated pHEMA control (left) and a decorin coated implant (right). It can be seen that collagen tissues which form the fibrous capsules (stained in blue) are visually similar in thickness below pHEMA implants which are light blue rectangles in the center of both images.
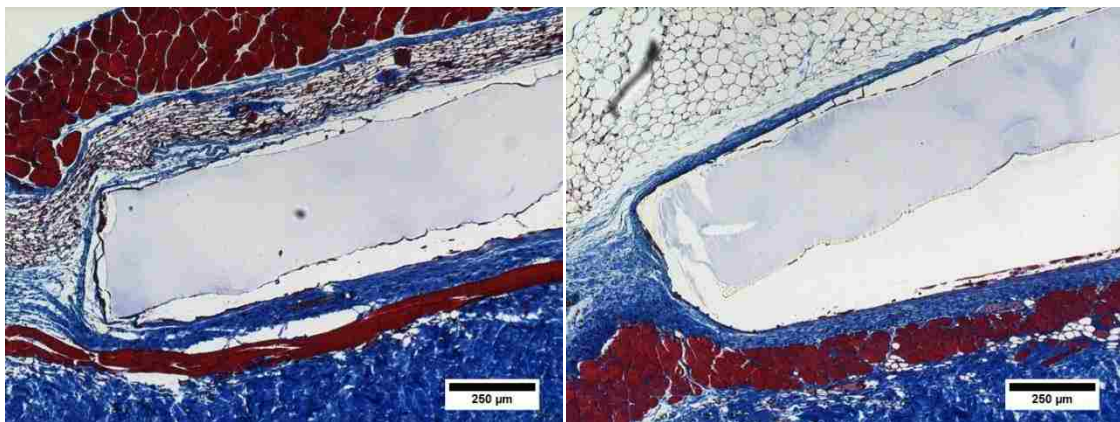
Figure 3.3. Masson's trichrome stained implant sections. Representative images of fibrous capsules present on uncoated pHEMA control samples (Left) and decorin coated samples (Right). Scale bar = 100µm

Overall, capsule thicknesses were not significantly different between groups. It was found in our lab that capsule thicknesses around implants tend to differ based on anterior or posterior location (unpublished data). In case capsule development was different on skin side vs. muscle side of implants, capsule measurements were separated by side of implant and by location. Capsules measured on the skin-side of implants from anterior locations in mice showed an increase in capsule thicknesses for decorin-coated implants as compared to controls, which was significant and in which the trend was maintained at the posterior location as well (Figure 3.4). Interestingly, the trend was reversed on the muscle side of implants at both locations though these trends were not statistically significant (Figure 3.5). If the data were not separated into skin side and muscle side, no significant differences were found in capsule thicknesses.

Numerous reports in the literature demonstrated reduced fibrosis and improved outcomes after decorin delivery. Administration of decorin in a rat arterial injury model[18], a rat model of kidney fibrosis[19], and a hamster model of lung fibrosis[20] all demonstrated lower levels of fibrosis. We thus expected to find a similar reduction in fibrous encapsulation as measured by either reduced capsule thickness or reduced capsule density in our wound healing implantation model.

Figure 3.4. Capsule thicknesses on skin side of implants. Capsule thicknesses were measured on Masson's Trichrome stained sections and compared between coated and uncoated samples at both anterior and posterior implant locations. * $p < 0.05$
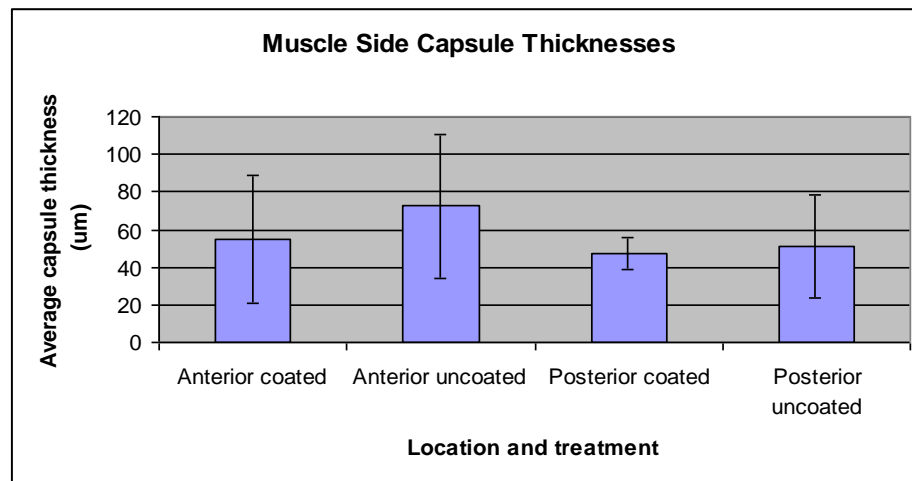
Figure 3.5. Capsule thicknesses on muscle side of implants. Capsule thicknesses measured on Masson's Trichrome stained sections and compared between decorin-coated and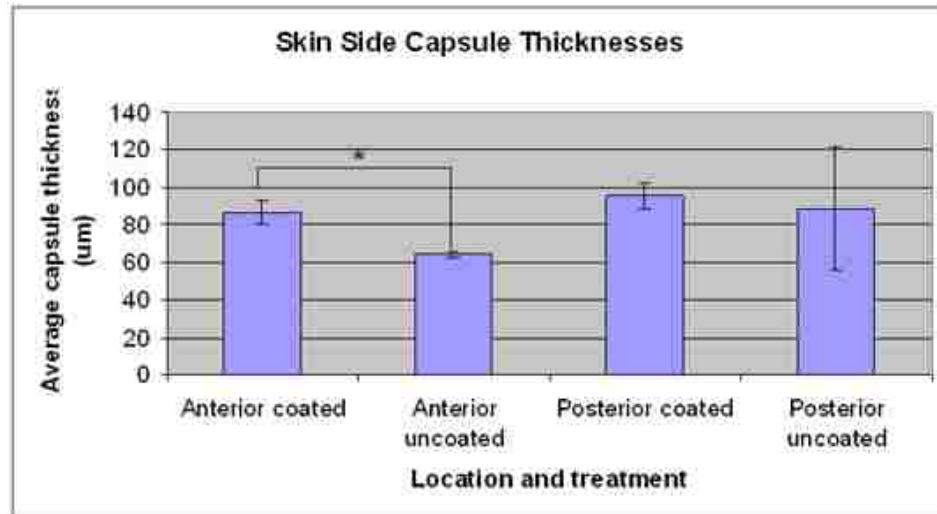 uncoated control samples at both anterior and posterior implant locations. No significant differences in capsule thickness were found on muscle side of implants.

The presentation of decorin on implant surfaces was designed to optimize efficacy of the coating. Collagen-bound decorin has been shown to retain its TGF-β binding activity, and collagen-bound decorin has also demonstrated reduced endocytosis[112]. Thus in attaching decorin to our surface via a collagen affinity coating we retain decorin's ability to bind TGF-β and reduce degradation of the coating at the implant site thus increasing the duration of time in which the coating can remain effective. The mechanism of decorin's ability to inactivate TGF-β is not fully understood but is believed to either sequester the molecule in the ECM[94] or clear it from the area, likely through the kidneys[78]. By presenting decorin on a collagen affinity coating, decorin would still have the ability to either sequester TGF-β at the implant site and prevent it from binding to its receptors, or clear the molecule from the area. It was for these numerous benefits that decorin was presented at the surface of these implants on a collagen affinity coating. Surprisingly, coated surfaces did not reduce fibrous encapsulation as expected. Overall, the decorin coating demonstrated no significant difference in either capsule thickness or density as compared to uncoated controls. Only when the data were separated by location and skin vs. muscle side of implant did a significant difference emerge, and it was a slight increase in capsule thickness for coated samples. This result contradicts the positive reduction in fibrosis in numerous other animal models[18-21]. This difference may be due to differences in decorin quantity, duration of decorin presence at the implant site, or that decorin may illicit a different response in an implant encapsulation model as compared to a simple injury model or fibrotic disease model.

Assessment of angiogenesis

Paraffin embedded sections were evaluated for endothelial cells though immunohistochemistry for MECA-32. There were little to no lumen structures present within capsules surrounding both pHEMA control implants and decorin control implants. The only visible lumen structures present on labeled sections were around the periphery of capsules within native mouse tissues. Thus full quantification of these results was not conducted. Representative images of MECA-32 labeled sections are given in Figure 3.6 with an uncoated pHEMA control (right) and a decorin coated implant (left). Studies have demonstrated both inhibition of angiogenesis and enhancement of angiogenesis from addition of decorin, and thus angiogenesis was measured to determine if decorin had a strong effect in a fibrous encapsulation model. Results indicate that a monolayer of decorin at the surface of an implant neither significantly enhances nor inhibits vascularization of the fibrous capsule.
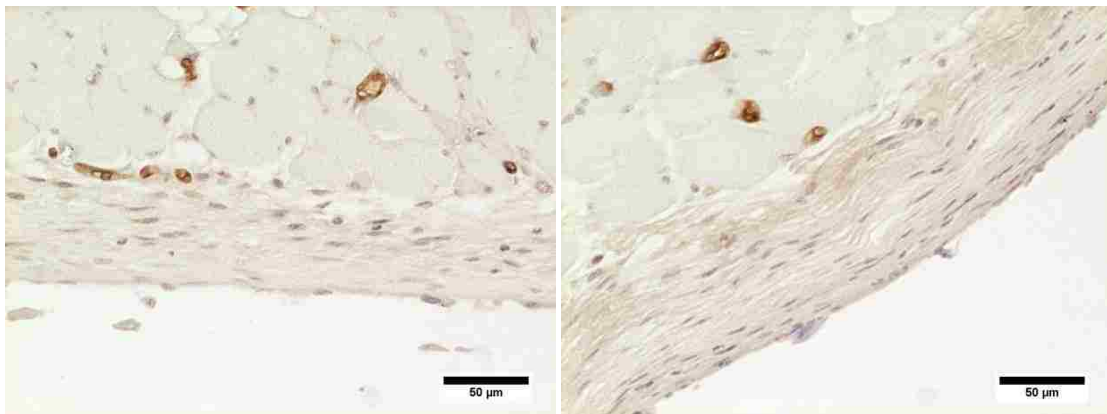
Figure 3.6. Representative images of MECA-32 staining for endothelial cells. Representative images of vessel evaluation present within capsules around uncoated pHEMA control samples (Left) and decorin coated samples (Right).

3.4 Conclusions

CAM assay

In order to evaluate and optimize our coating for improved healing *in vivo* we employed a chick chorioallantoic membrane (CAM) assay. The CAM assay is well established as a model for angiogenesis and has been reported to form fibrous capsules around implants. This model was evaluated as a potential fibrous encapsulation model based on lower cost and easier availability compared to traditional rodent models. Analysis of histological sections from assay samples demonstrated incomplete incorporation without measurable fibrous encapsulation. Our challenges with implant incorporation were in agreement with previous studies, however, we had the advantages of implanting only protein-coated samples of small diameter, which should have led to successful incorporation based on previous reports. In summary, we were able to conclude that the CAM assay produces a foreign body reaction, however, the small size of the fibrous capsule, limitations on implant size, and challenges with incorporation lead us to recommend against use of this model for assessment of fibrous encapsulation. For evaluation of angiogenesis and healing around micro sensors, the CAM assay has demonstrated success and the challenges we encountered do not indicate any relation to those more ideal applications for this model. Based on these findings we decided to move forward with *in vivo* evaluation of decorin-coated implants in a traditional rodent model.

Mouse subcutaneous implant model

A pilot study was carried out to evaluate fibrous encapsulation around decorin-coated implants as compared to uncoated pHEMA controls. Several controls were absent in this study to reduce animal number and search for an all-or-nothing response. It was found that coated surfaces did not reduce fibrous encapsulation as expected despite the fact that decorin had demonstrated positive reduction in fibrosis in numerous other animal models[18-21]. This difference may be due to a need for greater decorin quantity, a longer duration of decorin presence at the implant site, or that decorin may not play a significant role in formation of the foreign body capsule. This work was also conducted in a small pilot study which may have been underpowered, and thus small differences may not have been statistically significant. It is useful to note, however, that such small changes would not provide the large reduction of fibrous encapsulation which would be necessary for clinical use. Certainly, a greater understanding of the role decorin plays in fibrous encapsulation and the foreign body response is needed. To address the concerns of insufficient quantities of decorin, or need for increased duration of decorin presence, in a subsequent chapter decorin is overexpressed at the implant site. This delivery method enables an increase in decorin quantity far above what one could attach in a monolayer at the surface and allows the duration of decorin presence to extend for the length of the implantation to provide a more thorough investigation of decorin effects on the foreign body response.

Chapter 4

Effects of Decorin Overexpression on

Foreign Body Response to Implants

4.1 Introduction

Pilot study results from decorin-coated subcutaneous implants indicated that a greater understanding of maximal effects that decorin can elicit at an implant site, specifically in terms of fibrous encapsulation and angiogenesis, were needed to direct future decorin therapies. Towards this end, the effects of a sustained excess of decorin at an implant site on fibrous encapsulation and angiogenesis were evaluated. This was accomplished through local cellular overexpression of decorin at the implant site.

Previously, primary rat aortic smooth muscle cells (ASMCs) which overexpress decorin were created and evaluated in a rat aortic balloon injury model[18]. These cells demonstrated overexpression of bovine decorin through the entire 28 day study and reduced ECM accumulation was found in tissue surrounding decorin-overexpressing cells compared to control cells. Due to the rat source of these cells, effects of decorin overexpression on healing around implants were evaluated in a corresponding rat model. It has been demonstrated in our lab that 100 μm pore-size scaffolds have significantly greater fibrous capsule formation and reduced angiogenesis as compared

to their 35 μm pore-size counterparts. 100 μm porous scaffolds are thus an excellent platform on which to evaluate the effects of decorin overexpression on fibrous encapsulation and angiogenesis *in vivo.* We fabricated porous polymer scaffolds with surface-immobilized collagen to promote cell attachment. We then optimized cell seeding of rat aortic smooth muscle cells which constitutively overexpress bovine decorin along with non-decorin-overexpressing control cells before implanting and evaluating healing. These cell-seeded scaffolds were optimized to deliver cell numbers which were previously found to be effective in reducing ECM accumulation[18]. This study enabled us to learn the maximum effects on healing we could expect from local administration of decorin.

The motivation for carrying out the decorin overexpression study was to obtain a greater understanding of the effects of decorin on fibrous encapsulation and angiogenesis, and thus be better able to optimize future decorin coatings or alternate therapeutic delivery of decorin around implants. Specifically, we would know whether or not to expect changes in capsule thickness, capsule density, and angiogenesis. Moreover, the decorin expression study was designed to ensure that addition of decorin locally at the implant site through a surface coating or other means had the potential to promote healing. Although the decorin overexpression study was carried out in a rat model, necessitated by the rat SMCs we used to overexpress decorin, evaluation of coated surfaces was carried out in a mouse implant model. No statistically significant differences in fibrous capsule thickness and angiogenesis were found between rat or

mouse models when tissues surrounding polymer implants were evaluated[113]. It is reasonable to believe that our mouse and rat models retained these similarities and thus are relevant models to compare results.

In order to gain a better understanding of the effects of a sustained excess of decorin on healing around an implant, we overexpressed decorin to effectively flood the system. Overexpression of bovine decorin from LDSN cells while not from LXSN cells was verified by Western blot. Seeding of cells onto porous pHEMA-co-MAA scaffolds coated with collagen was then optimized to maximize cell number and corresponding decorin output. LDSN-seeded scaffolds, LXSN-seeded scaffolds, and control scaffolds without cells were implanted subcutaneously in rats. Survival of these cells and sustained expression of decorin was demonstrated in the rat aorta over a 28 day period[18], and thus it was reasonable to expect these cells to survive for the entirety of our 28 day implant study. We assessed the healing response around cell-seeded scaffolds to determine effects of decorin on fibrous encapsulation, macrophage infiltration, and angiogenesis.

4.2 Materials and Methods

Cell culture

Primary rat aortic smooth muscle cells (ASMCs) stably transfected with the bovine decorin retrovirus LDSN and cells with LXSN retroviral vector alone were generously

provided by Dr. Tom Wight and Dr. Michael Kinsella (Hope Heart Institute, Seattle, WA). ASMCs were obtained from Fisher 344 rats[114] and transduced as previously described[18, 100, 115, 116]. Briefly, full length cDNA of bovine decorin (PG28) was inserted into the *Eco*RI site of the retroviral vector LXSN to create the retroviral vector for bovine decorin expression, LDSN. LDSN and LXSN were transfected into the packaging cell line PE501 and the virus produced was then used to infect a second packaging cell line PA317. PA317 cells were selected for G418 resistance in media containing 600 μg/ml of G418. Virus production was titered in NIH 3T3 TK⁻ cells and used to stably transduce Fisher rat ASMCs. Transduced ASMCs were selected using 800 μg/ml of Geneticin (G-418) in media alongside mock-transduced cells. Media was changed every 3 days during selection until mock-transduced cultures were dead, approximately 10-14 days. Cells were received at passage 8 after initial transduction. Cells were maintained in culture medium (high glucose DMEM containing 10% FBS, 1% antibiotic/antimycotic, 1% L-glutamine, 1% sodium pyruvate and 1% non-essential amino acids) and passaged every 5-7 days at 1:4 until used for experiments at passages 9-11.

SDS-Page and Western blot for analysis of decorin expression

LXSN and LDSN cells were cultured in growth medium in T-75 flasks until near confluence. Cell populations were then rinsed with warm PBS and serum-free growth medium was added. Cells were cultured an additional 24 hours and conditioned media was removed and run through a column containing DEAE Sephacel to concentrate and

purify proteoglycans. Samples were run on SDS-Page gels and evaluated via Western blots as described with some modifications[116]. Concentrated samples were run on a 4-15% SDS Page gel. The gel was then transferred to nitrocellulose for 1 hour using a Bio-Rad Transblot transfer apparatus. To probe for decorin, the membrane was blocked with blocking buffer (Tris buffer containing 2% BSA Fraction V and 0.05% Tween 20) for 2 hours and then incubated overnight at 4 C with an antibody against the core protein of bovine decorin (LF-94 generously provided by Dr. Larry Fisher, NIDCR, National Institutes of Health, Bethesda, MD) diluted 1:4000 in blocking buffer. The membrane was washed and then incubated with a goat anti-rabbit HRP-conjugated secondary antibody (diluted 1:10,000 in blocking buffer) for 1 hour followed by visualization with Western Blot Chemiluminescence Reagent Plus and development on light-sensitive film.

Preparation of porous scaffolds

Polymer scaffolds were created, coated with collagen to promote cell attachment and seeded with LXSN or LDSN cells. 100 μm porous scaffolds were prepared using a sphere templating technique described previously[51]. Briefly, poly-methyl methacrylate beads (PMMA, Vicki Peters) were size separated by sifting through sieves until a size distribution of 95.6-105.4 μm beads were obtained. The beads were then placed between microscope slides separated by 1 mm Teflon spacers and sonicated to obtain tight, regular packing of beads. Beads were then heat-sintered at 140°C for 24 hours to create a bead cake. This bead cake was infiltrated with a solution to create a

copolymer of HEMA and MAA (pHEMA-co-MAA) at a molar ratio of 19:1 and allowed to polymerize overnight. The polymerization solution contained 4.75 ml of 2-HEMA, 0.19 ml of MAA, 0.23 ml of TEGDMA, 1 ml of H_2O, 1.5 ml of Ethylene glycol, 0.25 ml of 15% sodium metabisulfite and 0.25 mL of 40% ammonium persulfate. After removing polymerized scaffolds from molds, surfaces were gently scraped with razor blades to remove nonporous skins which develop between the bead cake and the slide surface. PMMA beads were solubilized in acetone leaving behind a sphere-templated pHEMA-co-MAA scaffold of approximately 100 μm pore size. Three acetone solvent changes of at least 1 hour each per day for at least three days on an orbital shaker table were carried out to remove unreacted monomer from scaffolds. Scaffolds were then cut into disks of 6 mm diameter and 8 mm diameter for optimization of cell seeding and implantation.

SEM visualization of porous scaffolds

Scaffold disks were evaluated using scanning electron microscopy (SEM) for visualization of scaffold morphology and evaluation of pore geometry.   Disks were dehydrated under vacuum and cut in half using a razor blade on a liquid nitrogen cooled surface to preserve pore structure for cross section evaluation. Samples for SEM were Au/Pd sputter coated for 30 seconds at 3 angstroms per second (SPI Supplies, West Chester, PA). Images were taken at the Center for Nanotechnology (University of Washington, Seattle, WA) on an FEI Sirion field-emission microscope (Hillsboro, OR). A fixed working distance of 5 mm was used and scaffolds were

scanned at an accelerating voltage of 5 kV under high vacuum. The top surfaces of disks were evaluated to ensure uniform removal of polymer skins and availability of porous bulk materials to seeded cells. Additionally, cross sections of scaffolds were visualized to confirm uniform porosity, pore interconnect size, and expected spherical architecture.

Surface modification of porous scaffolds

Copolymerization of pHEMA with a 5% molar ratio of methacrylic acid (MAA) provided carboxyl functional groups on the surface which were available to react with 1-ethyl-3-(3-dimethyl aminopropyl) carbodiimide (EDC) and *N*-hydroxysuccinimide (NHS) to immobilize collagen. Rat-tail type I collagen (BD Biosciences) was covalently linked to scaffold surfaces using EDC/NHS to allow for cell attachment as described below. Scaffold disks were solvent exchanged from acetone to ethanol by three-30 minute changes of fresh 100% ethanol on an orbital shaker table. Disks were placed into tubes containing 1ml of 100% ethanol. Ethanol was removed and 1.5 ml of 0.1 M EDC, 0.2 M NHS solution in ethanol was added. After solution changes, the tubes were spun for a few seconds to help solutions infiltrate scaffolds. The EDC/NHS reaction proceeded for 1 hour at room temp on an orbital shaker. Following this reaction, the EDC/NHS solution was removed and 1.5 ml of 100μg/ml collagen in ethanol was added to each tube. Tubes were placed on a rocking table at 4 C and reacted for 30 minutes before solution was replaced with fresh collagen solution and reacted overnight on a rocking table at 4 C. Scaffolds were sterilized by soaking in

70% ethanol overnight. Scaffolds were then equilibrated to sterile PBS (three-30 minute changes) followed by media equilibration (two-30 minutes changes of fresh sterile media).

Optimization of cell seeding

Multiple cell seeding experiments were conducted in order to maximize the number of cells retained in collagen-coated porous scaffolds. Initial static seeding consisted of collagen-coated scaffolds placed into multiwell plates. Cells were seeded onto the wells at concentrations of 10,000 or 100,000 cells per 100 μl (10^5 or 10^6 cells/ml) and allowed to attach and migrate for 24 or 72 hours. Cell-seeded scaffolds were then fixed in modified Methyl Carnoy's fixative overnight at 4°C. Samples were then dehydrated, paraffin infiltrated, embedded and 5 μm sections were cut. Sections were stained with hematoxylin and eosin and 10x images were taken on a Nikon upright microscope to evaluate seeding efficiency. Subsequent seeding experiments altered seeding methods (centrifugation, wicking via capillary action, injection), seeding densities (10^4 - 10^7 cells/100 μl), culture times post seeding, and duplicate and triplicate seeding in the same scaffold. Seeding methods were optimized to obtain final quantities of at least 10^6 cells per well and finally a triplicate seeding protocol was selected. Cell suspensions of 10^7 cells/100 μl were first wicked through scaffolds via capillary action and allowed to attach for 24 h. Secondary seeding involved direct injection of cell suspension and 24 h attachment, and then a final seeding consisted of

wicking cell suspensions through scaffolds. Cell seeded scaffolds were cultured an additional 24 hours before implantation.

Cytotoxicity evaluation

The fibroblast cell line, NIH 3T3, was used according to ISO standard 10993-5 to evaluate cytotoxicity of implant materials made in the same batch as were implanted. Cells were seeded in 12-well TCPS plates in one ml of growth media (High glucose DMEM + 10% FBS + 1% l-glutamine + 1% sodium pyruvate) per well. Porous collagen-coated scaffold implants were incubated in growth media for 24 hours at a volume of 3 ml of media per 9 cm^2 of surface area (calculating surface area based on nonporous disk size). Latex punched from pipette bulbs with a 5 mm diameter biopsy punch was sterilized in 70% ETOH for 8 hours, rinsed in 40 ml DI water with 4 water changes after 15 minutes each, and then soaked in growth media overnight as a positive control. Media incubated in TCPS wells served as a negative control. Cells were cultured for one day in growth media and then the media was aspirated off, media from TCPS, collagen-coated scaffolds or negative control wells were then added to cell wells, and cells were cultured for an additional 48 hours. Cells were visualized under a microscope at 24 and 48 hours for signs of toxicity, and Alamar blue proliferation assays were run as quantitative measures of toxicity. Solutions were aspirated off of cell cultures and DMEM + 10% Alamar blue was added to each well, incubated for 4 hours until a color change appeared and read on a fluorescent plate reader.

Endotoxin evaluation

Threshold endotoxin testing was carried out using Cambrex Bioscience Limulus Amebocyte Lysate Pyrogent Plus kit according to manufacturer's instructions.

Subcutaneous implantation

Four male Fischer 344 rats per treatment group were used for implantation. All animal procedures were approved by the University of Washington IACUC (Institutional Animal Care and Use Committee). All survival surgeries were carried out with rats under isofluorane and with administration of eye gel to prevent drying. Rats were shaved from just below the shoulders to just above the tail, rubbed with Betadine to prepare the skin for surgery followed by ethanol to remove the Betadine.

Surgeries were performed on clean pads placed on a water circulating warming pad set to 37 C to prevent heat loss. Each rat was placed in the prone position and a dorsal incision made with a sterile scalpel just offset from the spine and about 2 cm in length. Blunt dissection scissors were used to create 3 separate subcutaneous pockets, one behind the forelimbs on each side and one in front of the hind limbs on one side of the rat. Both anterior and posterior implant locations received the same treatment implant and the second anterior pocket received a control scaffold which was not seeded with cells. After creation of each subcutaneous pocket, implants were placed deep into pockets to prevent migration toward the incision location during healing. Wounds were closed with wound clips and rats received 0.05 mg/kg of body weight of

buprenorphine, injected subcutaneously near the base of the tail or on the ventral side near the gut post-surgery. Rats were checked each day for seven days post-implant for signs of pain or alterations in behavior. Implants remained for a 28 day encapsulation study. Rats received standard rodent chow and water during the course of the 28 day study. In previous use of these cells in rats, immune suppression was not required nor were antibodies to bovine decorin produced during the 4 week study[18].

Sample explantation and tissue processing

After 28 days, animals were sacrificed and implants and surrounding tissues were removed. Tissue samples were fixed in Methyl Carnoy's fixative for 3 hours and 45 minutes per sample, paraffin embedded and 5 μm sections were cut for histological analysis.

Assessment of healing response around scaffolds

Paraffin sections were stained with hematoxylin and eosin (H&E) according to manufacturer's instructions. Images were obtained on a Nikon E800 upright microscope for assessment of overall inflammatory responses.

Assessment of seeded smooth muscle cells

Seeded LXSN and LDSN rat aortic SMCs were located by immunohistochemistry for the muscle protein desmin (Vector Labs). Paraffin embedded 5 μm sections were baked onto slides, deparaffinized in xylenes and rehydrated to ICC PBS. Sections were

peroxidase quenched with 3% hydrogen peroxide in methanol for 30 minutes during rehydration steps. Sections were then incubated with blocking buffer (4% normal goat serum in ICC PBS) overnight at 4° C, followed by incubation with mouse monoclonal antibody to desmin (1:20 in blocking buffer) for one hour at room temperature. Sections were washed with ICC PBS and incubated with biotinylated horse anti-mouse secondary antibody (1:400, Vector Labs) for 1 hour at room temperature followed by a streptavidin-peroxidase complex (ABC) for 30 minutes at room temperature. Sections were developed using SigmaFAST DAB for 1 minute and 30 seconds, dehydrated and coverslipped with Permount. Stained sections were visualized using brightfield microscopy.

Illustration of bovine and rat decorin presence

Presence of both overexpressed bovine decorin and native rat decorin was detected using polyclonal antibodies directed against the core protein of bovine decorin (LF-94) or rat decorin (LF-113, both generously provided by Dr. Larry Fisher, NIDCR, National Institutes of Health, Bethesda, MD)[117] as previously described with minor modifications[18]. Sections which were used with LF-94 and LF-113 antibodies were digested with chondroitin ABC lyase (ICN Biomedicals, 200 mU/ml in 0.1mol/l Tris-acetate, pH 7.3) for 1 hour at 37°C. Both LF-94 and LF-113 were diluted 1:1000 in ICC PBS + 4% normal goat serum. After washing with ICC PBS, sections were incubated with a biotinylated goat anti-rabbit secondary antibody (diluted 1:400) for 30 minutes followed by addition of a streptavidin-peroxidase complex (ABC) for 30

minutes at room temperature. Sections were developed using SigmaFAST DAB for 45 seconds, counterstained with hematoxylin, dehydrated and coverslipped with Permount.

Measurement of capsule thickness and density

Methyl Carnoy's fixed tissue sections were stained with Masson's trichrome according to manufacturer's instructions. Additional sections were stained with picrosirius red as described[118] for greater ease and accuracy in measuring capsule thickness and density. A Nikon E800 upright microscope was used to take 4x images of stained sections. Picrosirius red images for capsule measurements were obtained under circularly polarized light. Capsule regions were traced using Image J software, and capsule thicknesses were calculated as total area of traced capsule divided by length of area for an overall average. Capsule density was determined as a percent of total area using threshold tools.

Quantification of angiogenesis

Detection of endothelial cells was initially performed by immunohistochemistry for rat endothelial cell antigen (RECA-1, Santa Cruz Biotechnology). RECA-1 is a pan-endothelial marker and RECA-1 antibodies positively labeled adult rat endothelial cells which were negative with PECAM-1[119]. Paraffin embedded 5 μm sections were baked onto slides, deparaffinized in xylenes and rehydrated to ICC PBS. Sections were peroxidase quenched with 3% hydrogen peroxide in methanol for 1 hour during

rehydration steps. Sections were then incubated with blocking buffer (1.5% normal goat serum in ICC PBS) for one hour at room temperature, followed by incubation with RECA-1 (1:20 in blocking buffer) overnight at 4°C. Sections were washed with ICC PBS and incubated with biotinylated horse anti-mouse secondary antibody (1:400, Vector Labs) for 1 hour at room temperature followed by a streptavidin-peroxidase complex (ABC) according to manufacturer's instructions. Sections were developed using SigmaFAST DAB for 5 minutes, counterstained with hematoxylin, dehydrated and coverslipped with Permount.

An alternate technique for identifying endothelial cells was found to be necessary and subsequent analysis was performed using immunohistochemistry for biotinylated *Griffonia (Bandeiraea) simplicifolia* lectin I isolectin b4 (1:25 in ICC PBS, Vector Labs) for 30 minutes at room temperature. Sections were washed using ICC PBS with 0.05% Tween 20 followed by a streptavidin-peroxidase complex (Vectastain ABC) for 30 minutes at room temperature. Sections were developed using SigmaFAST DAB for 1 minute and 15 seconds, counterstained with hematoxylin, dehydrated and coverslipped with Permount. High magnification images were obtained and lumen structures were counted to quantifying angiogenesis. All counts were performed blinded.

Macrophage quantification

Mouse anti-rat CD-68 (AbD Serotec) primary antibodies were used to detect macrophages in tissue sections. Sections were blocked with 4% normal serum in ICC PBS overnight and incubated with CD-68 primary antibody (1:50 dilution) in blocking buffer for 1 h at room temperature. Following three PBS washes, sections were incubated with a biotinylated horse anti-mouse secondary antibody for 30 minutes at room temperature. Sections were then washed, incubated for 30 minutes with ABC and developed using DAB. Macrophage quantification was performed on non-counterstained sections using threshold tools in Image J and is reported as a percent of total area per high power field.

4.3 Results and Discussion

SDS-Page and Western blot for analysis of decorin expression

Conditioned media from cultures of LXSN and LDSN cells after 24 hours in serum-free conditions was run through a column containing DEAE Sephacel to concentrate and purify proteoglycans. Samples were run on SDS-Page gels and evaluated via Western blots. An antibody against the core protein of bovine decorin was used to confirm production of decorin by our LDSN decorin-overexpressing cells as well as lack of decorin presence in media from our LXSN control cells. LDSN cells have been shown to express intact (glycosylated) bovine decorin at approximately 30 μg/10^7 cells in 24 hours[100]. After digestion of our conditioned media with chondroitinase ABC, our

Western blot showed a positive decorin band at approximately 40 kD for our LDSN cells whereas in the lane containing our LXSN conditioned media this decorin band was absent (Figure 4.1).
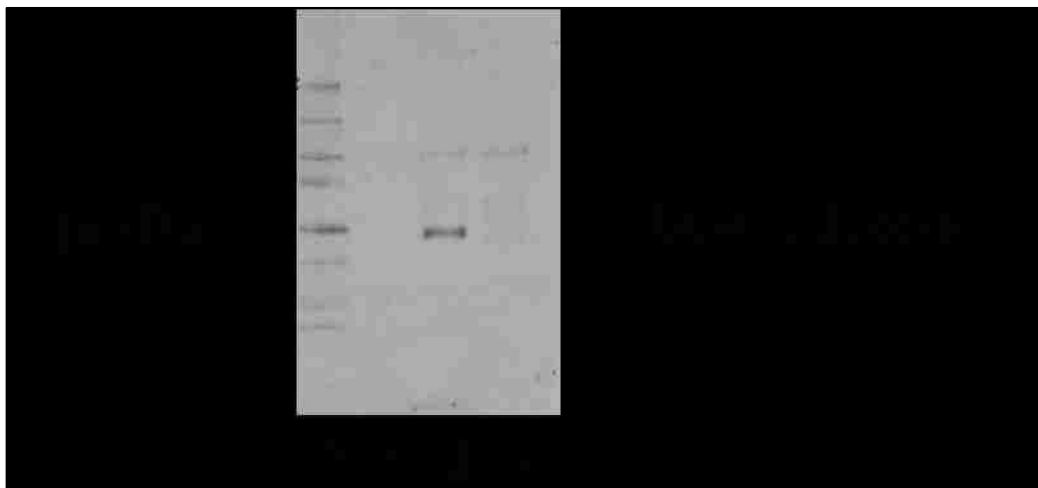
Figure 4.1: Western blot probed for core protein of bovine decorin. Positive band for bovine decorin core protein at approximately 40 kD can be seen in conditioned media from decorin-overexpressing LDSN cells (Lane 3) while this same band is absent in conditioned media from LXSN control cells (Lane 4). Lanes 1 and 2 are ladder and enzyme control, respectively.

SEM visualization of porous scaffolds

Scaffold top surfaces and cross sections were evaluated using SEM to ensure uniform porosity, spherical pore geometry, and that scaffold pores were interconnected. Unexpectedly, top surfaces of scaffolds demonstrated a layer of pores which were not interconnected with the bulk. However, scaffold cross sections showed uniform, spherical pores which were interconnected as expected. Representative images can be seen in Figure 4.2. It is clear that the typical skin which forms between the glass slides

and bead cake was successfully removed to reveal a porous layer. Further iterations of scaffold fabrication produced the same result with lack of porous interconnects between the surface pore layer and the bulk. We believe that during the sintering process, as the bead cake fuses to form what later becomes the pore interconnects, it shrinks and pulls away from the glass plate and allows an additional polymer skin to form along the top and bottom surface of the scaffold. This challenge was overcome by increasing the amount of scraping on both the top and bottom surfaces of infiltrated bead cakes. These final scaffolds were found in SEM to contain spherical, uniform, interconnected pores on surfaces and cross sections as seen in Figure 4.3.
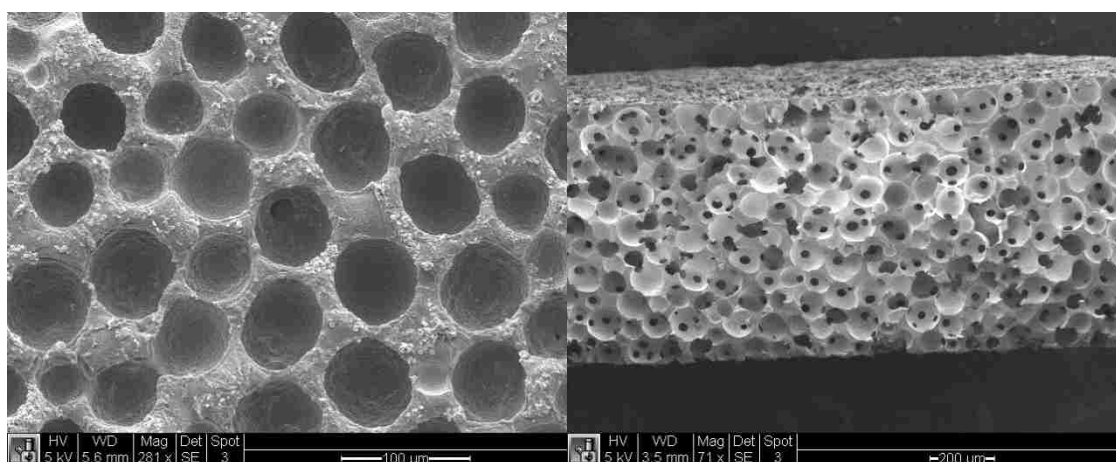

Figure 4.2: SEM images of porous scaffolds lacking interconnected pores on top surface. Representative SEM micrographs of porous pHEMA-co-MAA scaffolds demonstrating pores on top surface which lack interconnects to pores below (Left) and cross section with interconnected pores (Right).
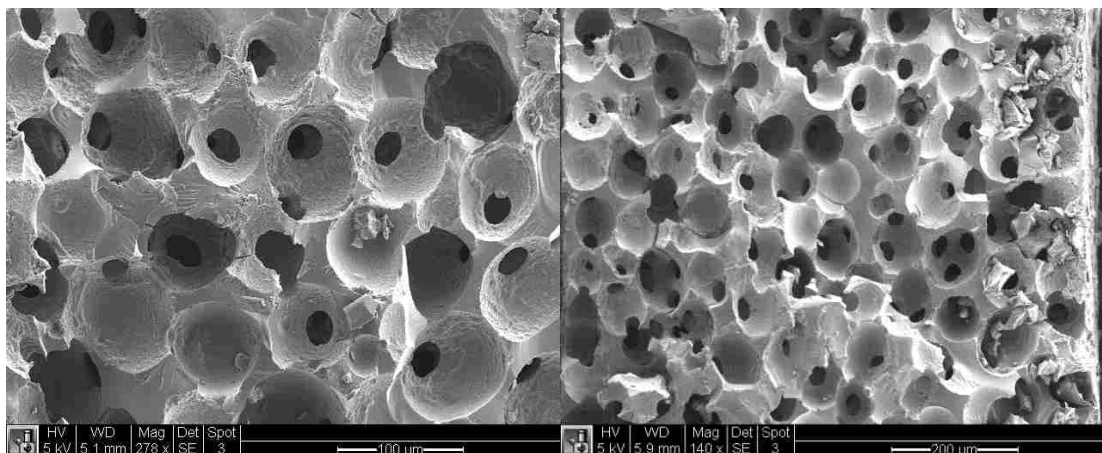
Figure 4.3: SEM images of porous scaffolds with uniform, spherical, interconnected pores. Representative SEM micrographs of porous pHEMA-co-MAA scaffolds demonstrating pore geometry of top surface (Left) and cross section (Right).

Optimization of cell seeding

As cells poorly adhere to pHEMA-co-MAA, surface modification with collagen was used to enhance cell attachment. Successful surface modification was presumed from successful attachment of cells to scaffold surfaces. After the initial cell seeding study, cells attached along the outer surfaces of the scaffold and proliferated outward, while very few cells migrated into the scaffold. While successful cell attachment and growth indicates successful collagen attachment, our ultimate goal was infiltration of cells to reach quantities equal to or greater than 10^6 cells per scaffold. This goal was set to implant comparable cell numbers to those used in the previously reported balloon injury model in which a reduction in ECM was demonstrated[18]. We attributed lack of cell infiltration into the scaffolds to be due to passive seeding methods, cell density, or cell culture times. We optimized delivery methods, cell suspension densities and culture times to maximize cell number within scaffolds and thus maximize decorin

production. We found that optimal cell seeded for these cells consisted of triplicate seeding in a single scaffold, and a combination of seeding methods including wicking by capillary action as well as direct injection of cell suspensions.

Cytotoxicity and endotoxin evaluation

All samples used in this study tested negative for endotoxin and thus have endotoxin levels under the 0.06 EU detectable level. Additionally, scaffolds demonstrated no cellular toxicity and were able to be used for implantation.

Assessment of healing response around scaffolds

Paraffin sections were stained with H&E for assessment of inflammatory response. Paraffin sections stained with H&E demonstrated a robust inflammatory response characterized by large amounts of cell infiltration which looked similar between LDSN seeded scaffolds, LXSN seeded scaffolds, and control scaffolds (Figure 4.4).

LDSN   LXSN
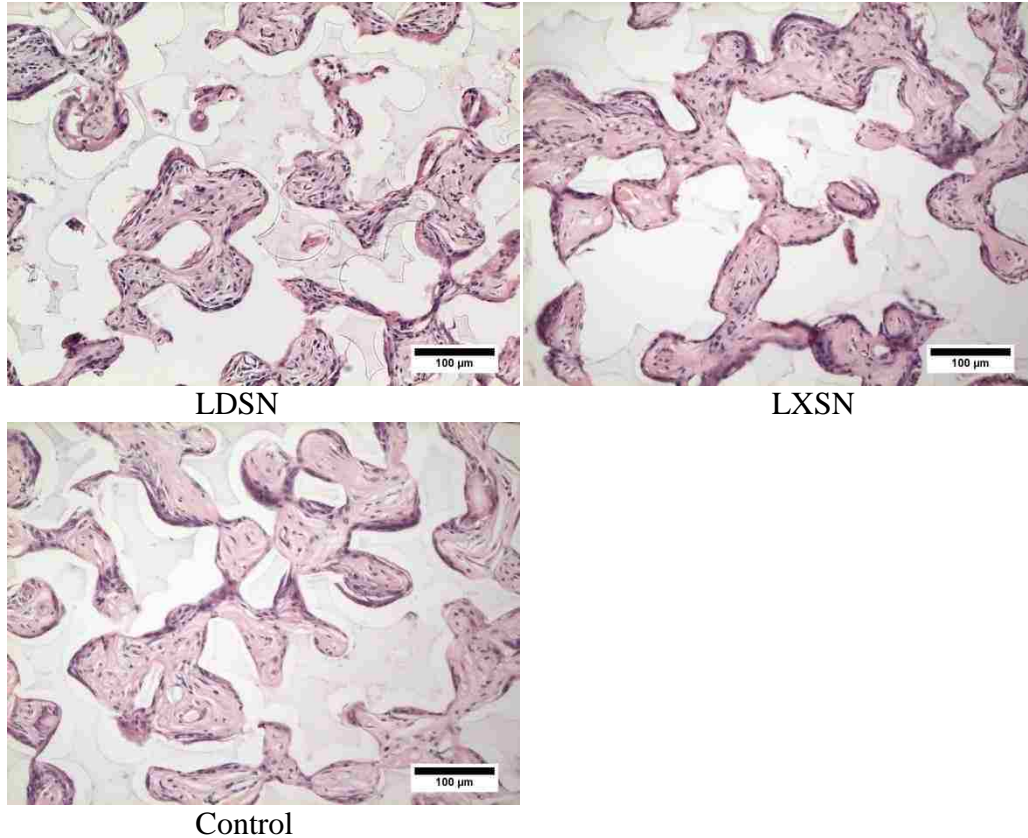
Control

Figure 4.4. Representative images of H&E stained tissue sections. Similar amounts of cell infiltration can be seen in decorin-overexpressing LDSN cell-seeded scaffolds (Top left), LXSN cell-seeded scaffolds (Top right) and control scaffolds which were implanted without cells (Bottom left).

Identification of seeded smooth muscle cells

In order to confirm that our seeded smooth muscle cells were retained within scaffolds

four weeks post-implant, we stained for the protein desmin. Successful retention of our

seeded smooth muscle cells was indicated by the large presence of desmin-positive

cells within our cell-seeded porous scaffolds and not our control scaffolds as seen in

Figure 4.5.As our implanted cells were the same Fisher rat source as our host animals,

we can only presume from the strong presence of positive cells in seeded scaffolds as

compared to control scaffolds that our cells are present. It has been shown that some

types of myofibroblasts may also express desmin and this likely explains the presence of a very few positively stained cells in control scaffolds. Further evidence in support of our seeded smooth muscle cells being retained in scaffolds was given by the fact that in cell-seeded scaffolds, as we sectioned through our scaffolds, the quantity of desmin positive cells varied. This indicated some differences in cell seeding densities throughout scaffolds. With control scaffolds, however, consistently very few cells stained positive regardless of where along the length of our scaffold we sectioned.

LDSN   LXSN

Scaffold Control   IgG Control

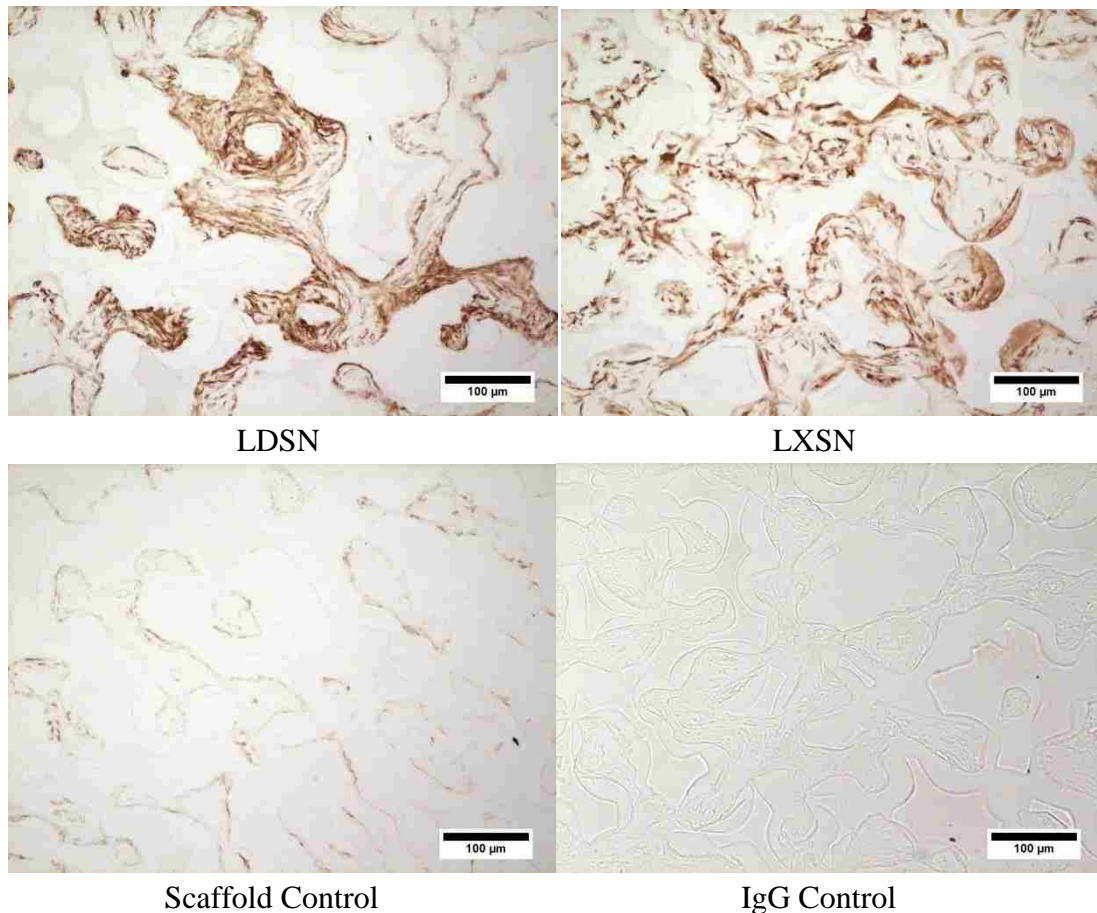**Figure 4.5. Representative images of desmin positive stained cells.** The large number of desmin positively stained cells in LDSN scaffolds (Top left) and LXSN scaffolds (Top right) as compared to very little staining in control scaffolds (Bottom left), and none in IgG controls (Bottom right) indicate that cells seeded in scaffolds were retained during the duration of the four week implantation.

<u>Illustration of decorin presence</u>

In support of LDSN cells and LXSN cells being retained in scaffolds four weeks post implant and to further confirm decorin presence at the implant site, an antibody directed against the core protein of bovine decorin was used (LF-94). This polyclonal rabbit antibody has inherent challenges with background and much optimization was performed to reduce background staining. As seen in Figure 4.6, a light amount of background staining is seen in all images. However, darker brown positive staining for bovine decorin can be seen in LDSN seeded scaffolds whereas in LXSN and control scaffolds this positive staining is absent. Demonstration of decorin overexpression further supports previous evidence that seeded SMCs remained in scaffolds during the duration of the 28 day study. Further, these findings illustrate that seeded LDSN SMCs produced decorin and decorin was retained within scaffolds. These results agree with previously reported data in which these same decorin-overexpressing cells survived and successfully produced decorin at the end of a 28 day balloon injury study[18].

LDSN

LXSN

Scaffold Control

Serum control
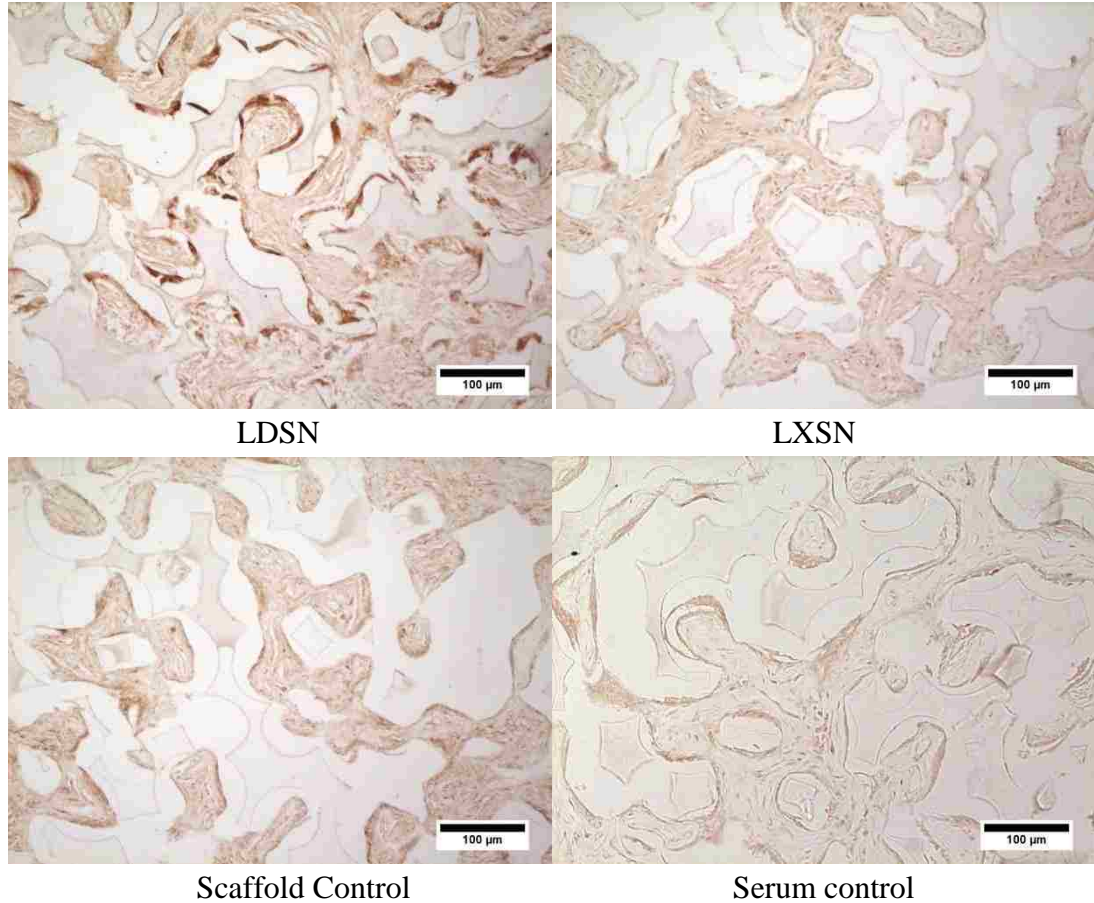
Figure 4.6. IHC images stained for bovine decorin. Tissue sections were stained using an antibody directed against the core protein of bovine decorin (LF-94). Light background staining appears in all images and dark brown positive staining is present in LDSN scaffolds (Top left) but is absent in LXSN seeded (Top right), control scaffolds (Bottom left), and normal rabbit serum control (Bottom Right).

Measurement of capsule thickness and density

Capsule thicknesses were initially visualized on Masson's trichrome stained sections as seen in Figure 4.7. Capsule densities on these images were obtained by separating images into color channels, selecting the blue channel, tracing the capsule, and taking a threshold of the stained area within the traced region. Capsule traces excluded edges to prevent edge effects from factoring into the analyses. The presence of black nuclei and

red cytoplasm within capsules affected threshold results and thus picrosirius red staining was conducted to improve accuracy of capsule measurements (Figure 4.8). Capsules were again traced taking care to exclude edge effects and the thicknesses were calculated as the total area of the traced capsule divided by the capsule length. As seen in Figure 4.9, no significant differences in capsule thicknesses were seen between LDSN, LXSN and control scaffold capsules. Images were then separated into color channels and capsule densities were measured using threshold tools to obtain percentages of total capsule area. Similarly to thickness results, no significant differences in capsule densities were found between LDSN, LXSN, and control scaffold capsules (Figure 4.10).

LDSN

LXSN

Control
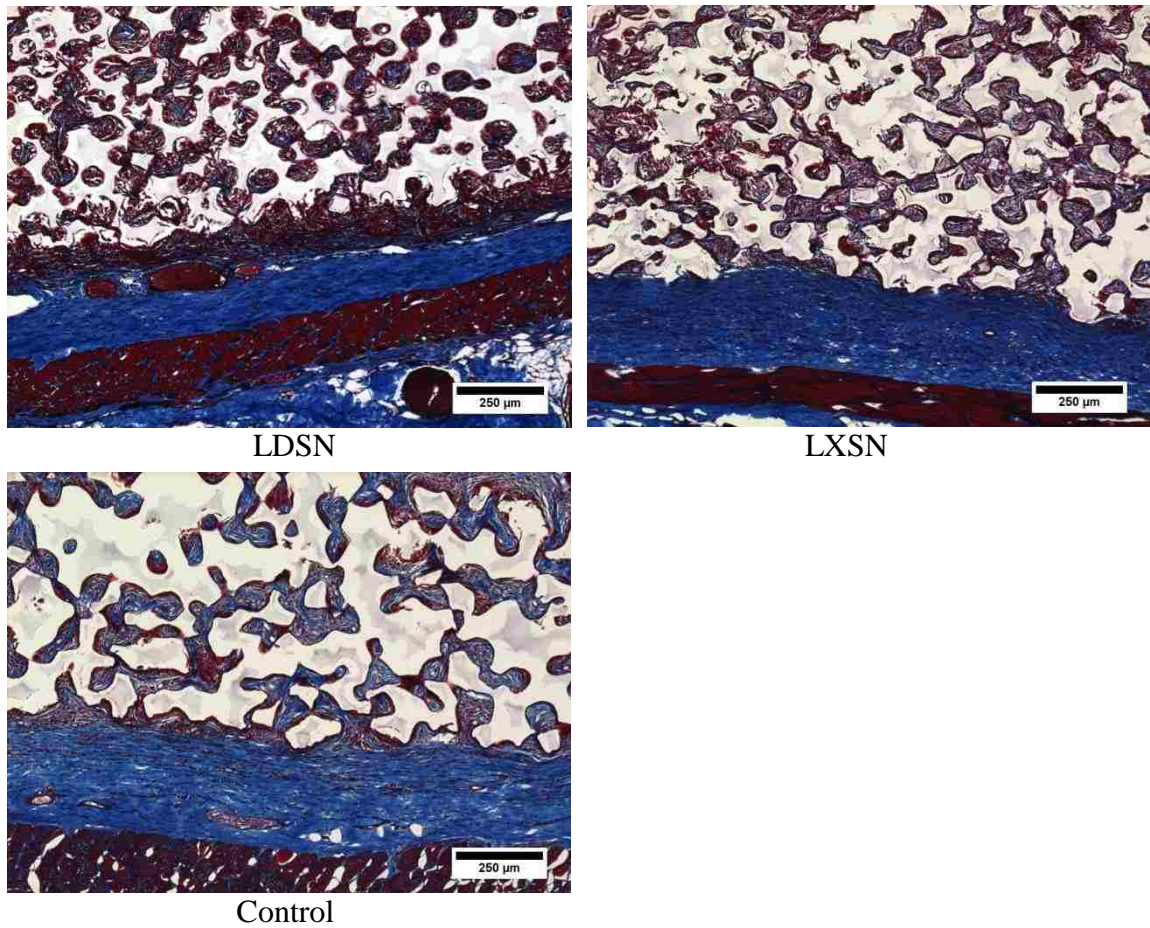
Figure 4.7: Representative images of Masson's trichrome stained tissue sections. Masson's trichrome images for evaluation of capsule tissue surrounding decorin-overexpressing LDSN cell-seeded scaffolds (Top left), LXSN cell-seeded scaffolds (Top right) and control scaffolds which were implanted without cells (Bottom left).

BRIGHTFIELD   CIRCULAR POLARIZATION

LDSN

LXSN

Control
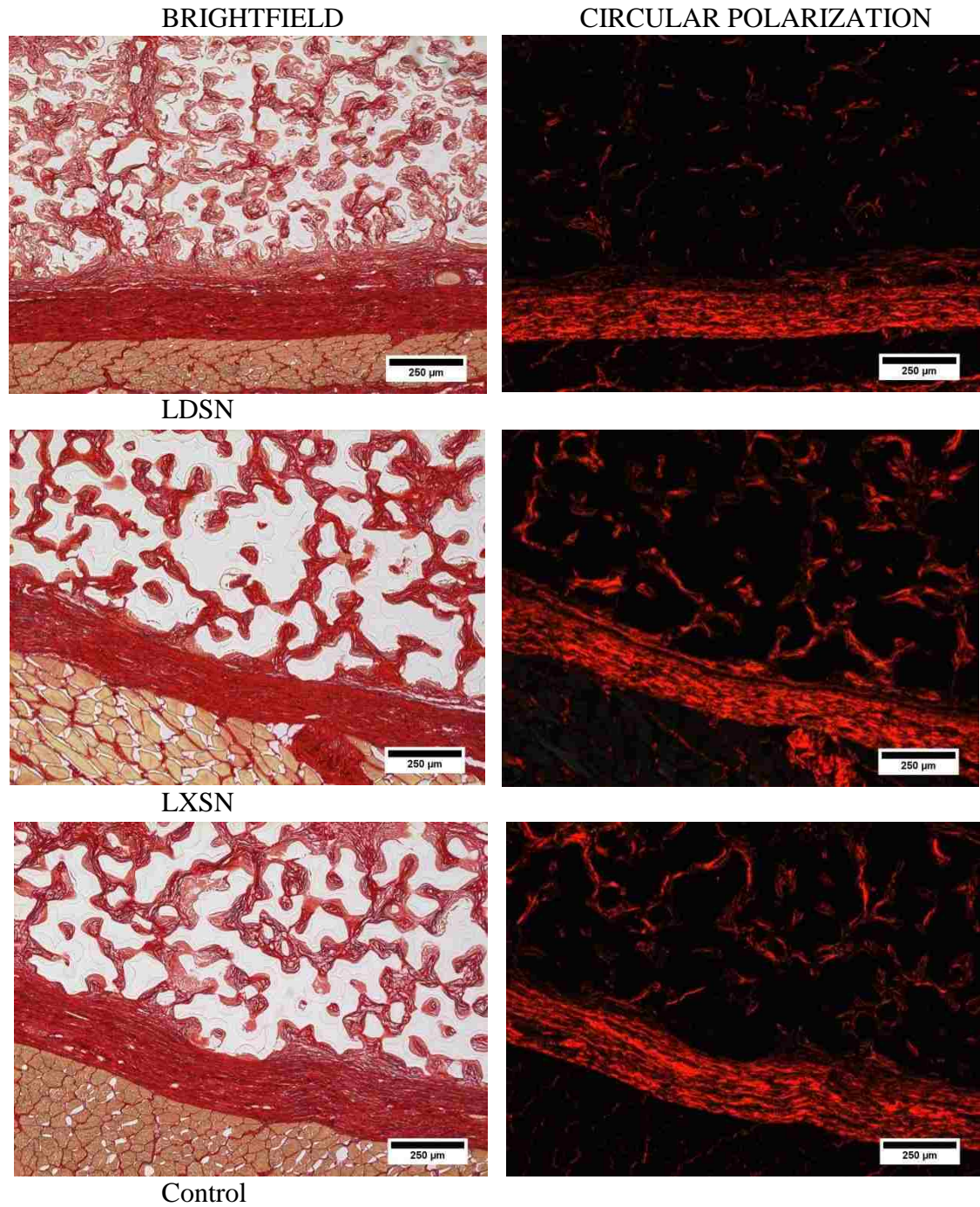
Figure 4.8: Representative images from picrosirius red stained tissue sections. Picrosirius red images taken in brightfield (Left column) or under circularly polarized light (Right column). Images show capsule tissue surrounding decorin-overexpressing LDSN cell-seeded scaffolds (Top), LXSN cell-seeded scaffolds (Center) and control scaffolds which were implanted without cells (Bottom).
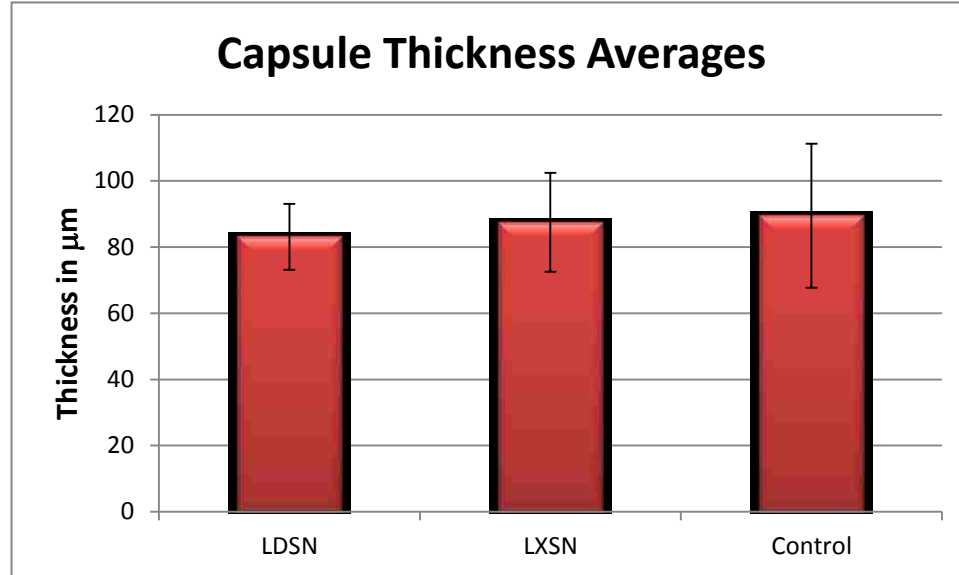
Figure 4.9: Capsule thickness measurements around porous scaffolds. Capsule thicknesses were calculated from picrosirius red stained tissue sections by tracing the scaffold in Image J and dividing the total area of a scaffold by the length of the scaffold to provide an average thickness. No significant differences were found in capsule thicknesses between LDSN, LXSN, and control scaffolds.

Figure 4.10: Capsule density measurements around porous scaffolds. Capsule densities were measured around porous scaffolds on picrosirius red stained tissue sections using Image J threshold tools and are reported as a percentage of total area. No significant differences were found in capsule densities between LDSN, LXSN, and control scaffolds.

The lack of effect of decorin overexpression on fibrous capsule thickness and density was a surprising result considering the support in the literature for a reduction in fibrosis in several other animal models[18-21]. In an arterial injury model ut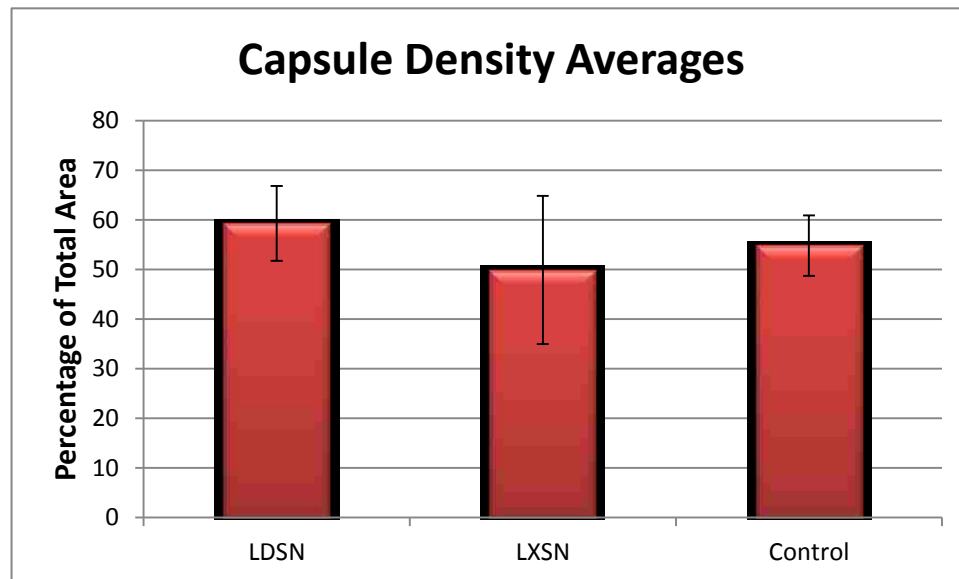ilizing this same cell type for overexpression of decorin, and in similar quantities as used here, a reduction in ECM area was found[18]. One notable difference between the use of decorin to reduce collagen deposition in these successful models and the lack of effect in our model is the presence of a foreign body at the wound site. This chronic stimulation of an inflammatory response leads to a distinctly different wound healing environment. Although the majority of studies in the literature report inhibitory effects of decorin on TGF-β activity, some researchers have found that decorin stimulates TGF-β activity[93] or has little effect on its activity at all[120]. It was suggested that low concentrations of decorin may stimulate TGF-β activity whereas higher concentrations used in other studies may inhibit activity[93]. However, in an excisional model of scar tissue formation, even high concentrations (100-200 μg/day over 11 days) of injected decorin did not reduce scar tissue formation as compared to controls[121]. When a targeting peptide was fused with decorin, the biological activity was enhanced both *in vitro* against TGF-β and *in vivo* by reducing scar tissue formation[121]. Notably, this targeting compound was effective in reducing scar tissue at concentrations of 40-80 μg/day over 11 days, which is less than half of the concentrations at which administration of decorin alone had no noticeable effect[121]. The authors attribute enhanced efficacy of the targeting compound with accumulation at the wound site, however, the increased

activity against TGF-β*in vitro* would suggest enhancement of biological activity in addition to simply accumulation at the wound site.

Quantification of Angiogenesis

Tissue sections were initially stained for endothelial cells using a RECA-1 primary antibody. These sections demonstrated incomplete identification of endothelial cells as seen in Figure 4.11. On different regions of a single section, some lumen structures would be nicely identified by the clear brown color while adjacent vessel structures would be entirely without stain. Because of these incomplete results, angiogenesis was instead quantified on tissue sections which were stained for isolectin b4. These sections gave a more robust and complete staining for endothelial cells as seen in Figure 4.12. Although this procedure also identifies macrophages[122], we were able to accurately quantify angiogenesis by counting only clearly identifiable vessel structures in our images. As shown in Figure 4.13, no significant differences in number of lumen structures were found between LDSN, LXSN, and control scaffolds.
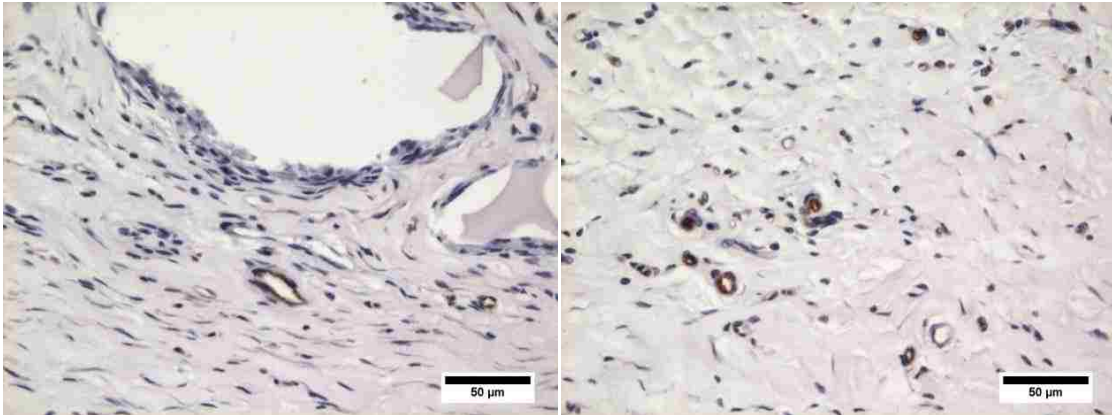
Figure 4.11: Representative images of RECA-1 IHC stained sections. Incomplete staining of lumen structures was found using RECA-1 primary antibody to detect endothelial cells. Although some endothelial staining nicely stained positive in brown, some clearly visible lumen structures should have stained positive and are completely unstained by RECA-1. Hematoxylin nuclear counterstain (blue).

<div align="center">LDSN   LXSN</div>

<div align="center">Control</div>
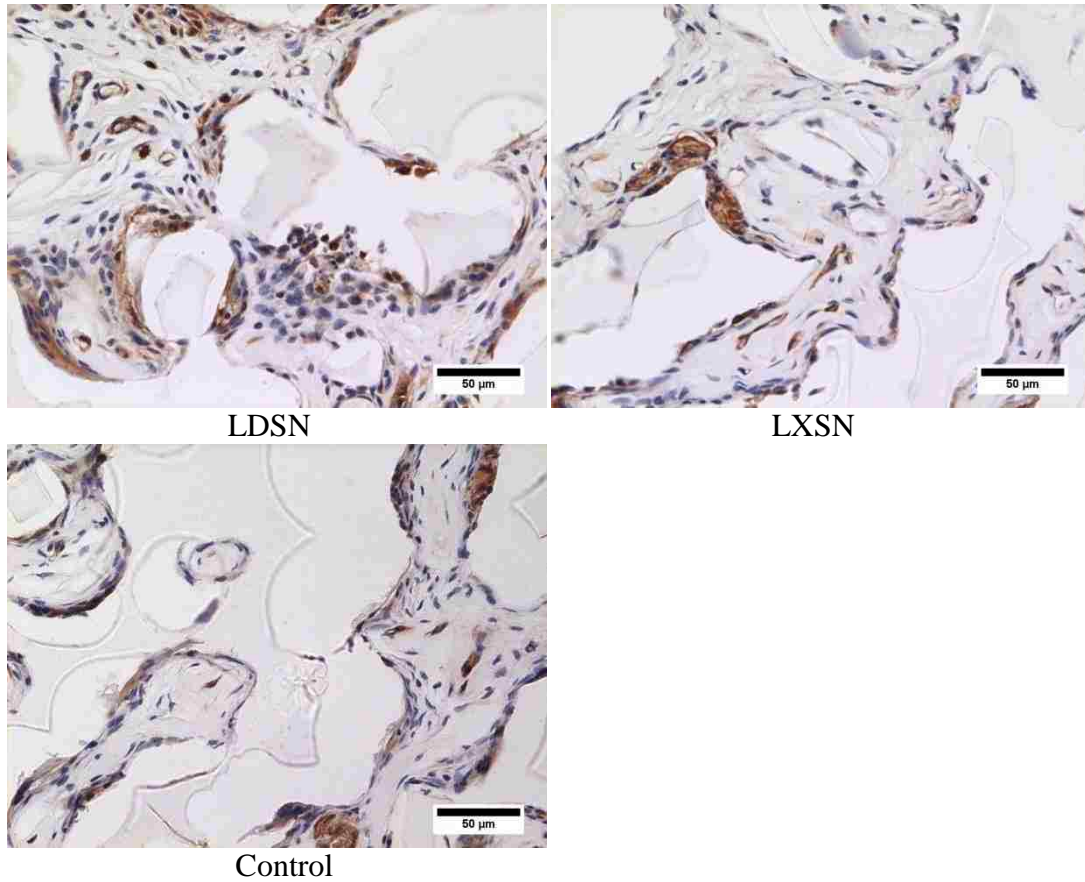
Figure 4.12: Representative images of isolectin b4 stained sections. Sections stained for isolectin b4 showed clear identification of lumen structures and more complete staining for endothelial cells along with staining of macrophages. Cell nuclei were counterstained with hematoxylin in blue.
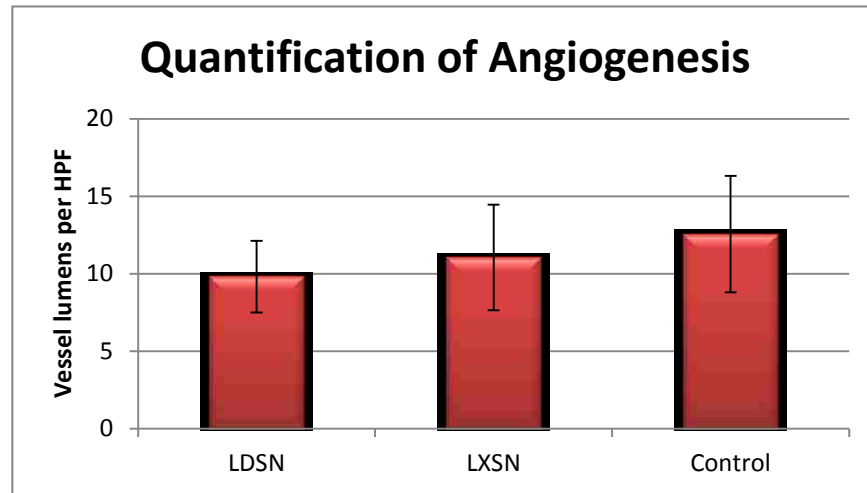
Figure 4.13: Quantification of blood vessels within porous scaffold. Vessel lumen structures were quantified within porous scaffolds on isolectin b4 stained sections. No significant differences were found in quantities of vessel lumens between LDSN, LXSN, and control scaffolds.

Macrophage quantification

An antibody directed against CD-68 was used to detect macrophage infiltration and compare between LDSN seeded, LXSN seeded and control scaffolds. Representative images of macrophages identified with CD-68 are given in Figure 4.14. Macrophage positive staining was primarily found at the periphery of the pores, along scaffold surfaces. Macrophage quantification was performed using non-counterstained images to prevent stained nuclei from contributing to the measurements. Macrophage quantities are reported as a percentage of total area in each high power field. We found that there were no significant differences in the amount of macrophage infiltration within LDSN, LXSN and unseeded scaffolds as seen in Figure 4.15.These results indicate that decorin does not appear to have a great effect on the quantity of macrophages present at an implant site four weeks post implantation.

LDSN

LXSN

Control
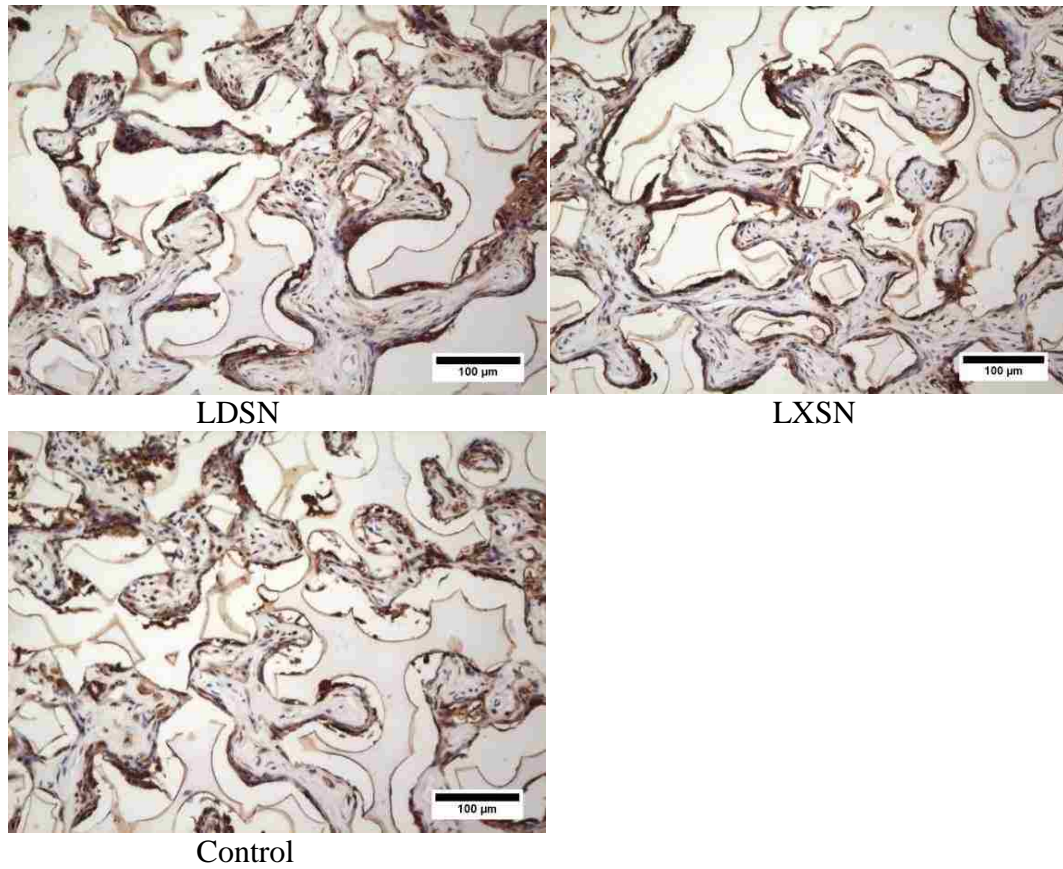
Figure 4.14. Representative images of CD-68 staining for macrophages. Images demonstrating macrophage presence within porous scaffolds using antibody against CD-68 and counterstained with hematoxylin. LDSN seeded scaffolds (Top left), LXSN seeded scaffolds (Top right), and control scaffolds (Bottom left) all show positive staining for macrophages along the polymer surfaces at the periphery of pores.
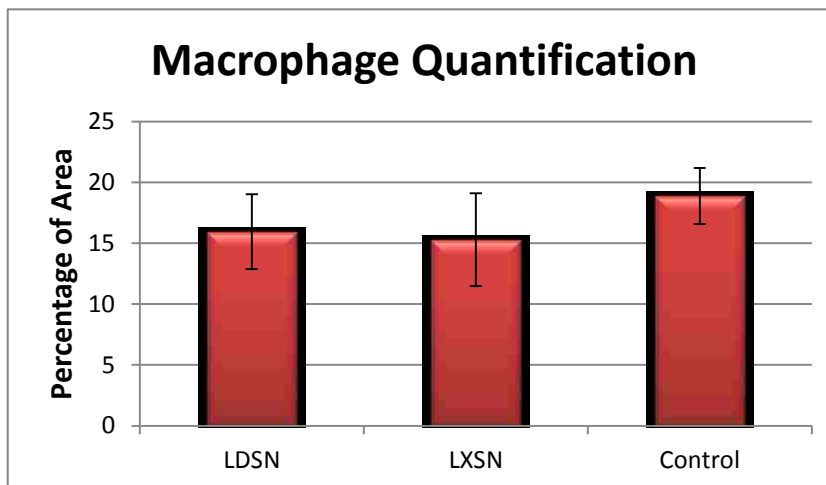
Figure 4.15. Macrophage quantification within porous scaffolds. Amount of macrophage infiltration within porous LDSN, LXSN, and control scaffolds were quantified using threshold tools and are given as a percentage of area per high power field (HPF).

4.4 Conclusions

For this work, porous pHEMA-co-MAA scaffolds were created, surface modified for cell attachment, seeded with LDSN and LXSN cells, and implanted subcutaneously for 28 days in the backs of rats. The goal was to elucidate the role that decorin plays in the foreign body response to biomaterials. We evaluated fibrous capsule thickness, capsule density, angiogenesis, and macrophage infiltration to determine differences between decorin-overexpressing scaffolds and control scaffolds. Unexpectedly we found that decorin overexpression did not elicit any significant differences in biological responses measured. There were no significant differences between decorin-overexpressing scaffolds and control cell seeded or unseeded scaffolds in terms of capsule thickness, capsule density, angiogenesis, or macrophage quantities. To ensure that decorin was present within decorin overexpressing scaffolds as expected, we

confirmed decorin overexpression through Western blot prior to implantations, and used immunohistochemistry to indicate that the smooth muscle cells which were seeded into scaffolds were present and that bovine decorin was located within scaffolds. This confirmation of decorin presence leads us to conclude that decorin overexpression does not dominate changes in foreign body capsule formation, angiogenesis and macrophage infiltration of porous implants. Low animal numbers used in this study may not have provided adequate power to demonstrate significance in small differences between groups. Despite this fact, differences great enough to provide a therapeutic benefit should have been detectable using this sample size. This indicates that decorin may not dominate these processes at the implant site. This study allowed us to determine the effects that essentially flooding the system with decorin had on fibrous capsule formation and angiogenesis, and led us to believe that local application of bovine decorin is not a promising therapy to promote healing around implants.

The *in vivo* model successfully developed in this chapter provided a novel delivery method for cellular overexpression systems. This system combined sphere-templated porous scaffolds which have controllable pore, pore throat and scaffold dimensions with cells which were transduced to overexpress a molecule of interest. In this case, decorin was our proteoglycan of interest, but this system could be used to explore effects of other proteins and proteoglycans of interest in the future. This work overcame scaffold fabrication and cell seeding challenges to deliver the desired

proteoglycan of interest at the implant site. We were able to demonstrate presence of both our seeded cells and decorin, 28 days post implant. Thus a promising means of delivering cell overexpression systems was created.

Chapter 5

Conclusions and Future Directions

5.1 Summary of Thesis Work

The work described in this thesis demonstrated the successful creation and characterization of a novel decorin surface coating. This coating enabled us to present decorin at the surface of a biomaterial in a mode similar to that found in the body, through natural binding to type I collagen. The collagen affinity coating has broad applicability for attachment of a wide variety of biological molecules that bind to collagen in the body as well as attachment of synthetic collagen-binding peptides, proteins, and peptidoglycans. This created a very promising platform onto which our decorin coating was created.

This work further evaluated the chick chorioallantoic membrane, an alternate model for assessment of fibrous encapsulation of biomaterials. The chick chorioallantoic membrane assay is a well-established angiogenesis assay which has also been reported to develop fibrous tissue surrounding sensor implants[105, 107, 108, 111]. This model had the potential advantages of reduced cost, reduced healing time and greater availability over standard rodent implant models. However, despite the success of the chick chorioallantoic membrane model for assessing healing responses using biological sensors[111], it was found that this model was less desirable than rodent models in terms

of histological analysis of tissue responses. In order to be implanted into the CAM model, implants needed to be considerably reduced in size compared to those allowable for rodent models both for survival of chick embryo and for incorporation of implants. Additionally, implants are restricted to materials and surface chemistries which allow for incorporation[105, 108]. Furthermore, although we successfully optimized our samples to be below the allowable implant size for embryo survival and protein-coated our samples to enhance incorporation, challenges of full incorporation still remained. Even the sample that did incorporate provided a very limited FBR that would make it difficult to detect measurable differences between treatments in such a thin capsule. Rodent models have the advantages of accommodating larger implant sizes as well as greater similarities to humans that outweighs the advantages of a shorter healing time and slightly reduced cost of this avian model.

A novel decorin surface coating was then evaluated in a rodent model for reduction of fibrous encapsulation around a polymeric biomaterial. Poly-2-hydroxyethyl methacrylate disks were created and the surfaces were modified to attach the decorin coating. Coated and uncoated samples were implanted subcutaneously into the backs of mice for 28 days before explanting along with surrounding tissues, fixing, paraffin embedding and processing for histological analysis. The thicknesses and densities of fibrous capsules were measured on Masson's trichrome stained sections. Surprisingly, this decorin coating did not demonstrate a reduction in either thickness or density of fibrous capsules. Moreover, capsules on both coated and uncoated samples consisted

of dense collagenous tissue with no or very few vessel lumens as visualized through immunohistochemistry for endothelial cells. These findings led to the consideration of several possible options. One option was that not enough decorin was present on the surface of the coating and an increased quantity would elicit the desired healing response. Another option was that decorin was degraded at the implant site too rapidly to have an effect and that presence of decorin for a longer duration would enable a reduction in fibrous tissue formation. We set out to address both of these possible options by maximizing both the quantity and duration of decorin present at the implant site while using a source and mode of delivery which demonstrated successful reduction of fibrosis in another animal model. We chose to overexpress bovine decorin at the implant site to determine the maximal effects that a decorin surface coating could have at an implant site.

The initial step in determining the maximal effects decorin could have at an implant site was to design an implant model in which these effects could be evaluated. For this purpose, sphere templated porous scaffolds were created and surface modified to facilitate cell attachment. Fischer 344 rat aortic smooth muscle cells that were transduced to overexpress bovine decorin were then seeded onto these scaffolds. These decorin-overexpressing cells were previously shown to reduce matrix accumulation in an arterial injury model as compared to control cells transduced with vector alone[18]. Numerous cell seeding challenges were overcome in order to obtain the desired quantity of cells within scaffolds. A triplicate seeding method was ultimately found to

be most effective at maximizing cell numbers. Decorin production by LDSN decorin

overexpressing cells was verified, and as shown previously[18], provided continuous

release of decorin into the area surrounding the cells. Cell seeded and control scaffolds

were implanted for 28 days and at this time point, the seeded SMCs were found in the

scaffold explants. Successful cell survival is a known challenge in numerous *in vivo*

models including cardiac and pancreatic models[123-126]. Demonstrating both successful

cell survival as well as decorin presence *in vivo* after 28 days was exciting evidence for

creation of a successful model for evaluation of decorin effects on the FBR. Several

aspects of the FBR were evaluated including collagen capsule thickness, capsule

density, angiogenesis, and macrophage infiltration. Through the development of this

novel FBR model, we were able to discover that decorin overexpression does not seem

to dominate the development and organization of the fibrous capsule surrounding

implanted biomaterials.   These findings were surprising considering the numerous

reports of reduction in fibrosis and improved outcomes in alternative models of fibrosis

after decorin delivery[18-21]. However, these models are not implantation models and

thus do not involve the FBR. The unique advantage of the model developed in this

work is that cells may be transduced to overexpress alternate proteins of interest and

the effects of these proteins specifically on the FBR can be evaluated using this cellular

overexpression implant model.

Through this work, a novel biologically active surface coating was created and

characterized, further demonstrating applicability for the collagen affinity coating that

provided the platform for the coating. As the number of natural and synthetic molecules which can bind to type I collagen continues to increase, the same techniques used for the creation of the decorin coating can be applied to additional promising molecules to create future coatings. Further, a successful model was developed for evaluation of the FBR. The ability to successfully seed cells into porous scaffolds, demonstrate cell survival after 28 days *in vivo,* and verify delivery of a molecule of interest at the implant site provides a promising method for evaluation of a number of additional potential therapies for the FBR.

5.2 Future Directions

The successful development of a decorin surface coating may have relevant applications outside of fibrous encapsulation for which it was designed. Despite successes of this proteoglycan in numerous models of fibrosis, the role of decorin in fibrous encapsulation specific to the FBR is not well understood and has not been extensively studied. This work provides evidence that decorin may not be the most promising therapeutic to reduce fibrous encapsulation in the foreign body response. It is worth mentioning, though, that in other models where decorin has met with more successful outcomes, a decorin coating may provide a promising therapeutic. Decorin has been reported to suppress tumor formation through inhibition of pro-angiogenic genes[127] and has been studied heavily as a cancer therapeutic[128-133]. One could thus

envision that a decorin coating on mammary implants may add additional protection from tumor recurrence after mastectomies.

The contribution of this work is not simply the successful development of a decorin surface coating, but also further demonstration of the broad applicability of the collagen affinity coating platform. This coating platform allows for the attachment of numerous natural collagen-binding molecules as well as synthetic peptides that have been designed strategically to bind to type I collagen. One particular synthetic peptide was designed to mimic many of the properties of small proteoglycans like decorin, including the ability to bind to collagen and the presence of a dermatan sulphate side chain. This peptidoglycan has shown promise after injection *in vivo*[134] and ability of this molecule to improve healing as a surface coating via this collagen affinity coating platform will be explored in the future.

Further application of decorin coating could involve attaching novel decorin compounds that have demonstrated enhanced activity as compared to the native proteoglycan. The creation of a targeting peptide which was fused with decorin enhanced its biological activity *in vitro* against TGF-β and *in vivo* by reducing scar tissue formation[121]. Notably, this targeting compound was effective in reducing scar tissue at concentrations where administration of decorin alone had no noticeable effect. This novel compound could be presented at the surface of biomaterials via the collagen

affinity coating and decorin binding in the exact manner in which the decorin surface

coating was created, and could provide enhanced efficacy.

References

1. Espicom. The Medical Device Market: USA - Overview of the medical market in the USA; 2012. http://www.espicom.com/usa-medical-device-market

2. Tang L, Eaton JW. Natural responses to unnatural materials: A molecular mechanism for foreign body reactions. *Mol Med.* 1999;5(6):351-358.

3. Mikos AG, McIntire LV, Anderson JM, Babensee JE. Host response to tissue engineered devices. *Adv Drug Deliv Rev.* 1998;33(1-2):111-139.

4. Woodward SC. How fibroblasts and giant cells encapsulate implants: considerations in design of glucose sensors. *Diabetes Care.* 1982;5(3):278-281.

5. Djakoure-Platonoff C, Radermercker R, Reach G, Slama G, Selam JI. Accuracy of the continuous glucose monitoring system in inpatient and outpatient conditions. *Diabetes Metab.* 2003;29(2 Pt 1):159-162.

6. Garg S, Zisser H, Schwartz S, Bailey T, Kaplan R, Ellis S, Jovanovic L. Improvement in glycemic excursions with a transcutaneous, real-time continuous glucose sensor: a randomized controlled trial. *Diabetes Care.* 2006;29(1):44-50.

7. Danielson KG, Baribault H, Holmes DF, Graham H, Kadler KE, Iozzo RV. Targeted disruption of decorin leads to abnormal collagen fibril morphology and skin fragility. *J Cell Biol.* 1997;136(3):729-743.

8. Iozzo RV. Matrix proteoglycans: from molecular design to cellular function. *Annu Rev Biochem.* 1998;67:609-652.

9. Iozzo RV. The biology of the small leucine-rich proteoglycans. Functional network of interactive proteins. *J Biol Chem.* 1999;274(27):18843-18846.

10. Reed CC, Iozzo RV. The role of decorin in collagen fibrillogenesis and skin homeostasis. *Glycoconj J.* 2002;19(4-5):249-255.

11. Schonherr E, Sunderkotter C, Schaefer L, Thanos S, Grassel S, Oldberg A, Iozzo RV, Young MF, Kresse H. Decorin deficiency leads to impaired angiogenesis in injured mouse cornea. *J Vasc Res.* 2004;41(6):499-508.

12. Schonherr E, O'Connell BC, Schittny J, Robenek H, Fastermann D, Fisher LW, Plenz G, Vischer P, Young MF, Kresse H. Paracrine or virus-mediated induction of decorin expression by endothelial cells contributes to tube formation and prevention of apoptosis in collagen lattices. *Eur J Cell Biol.* 1999;78(1):44-55.

13. Tralhao JG, Schaefer L, Micegova M, Evaristo C, Schonherr E, Kayal S, Veiga-Fernandes H, Danel C, Iozzo RV, Kresse H, Lemarchand P. In vivo selective and distant killing of cancer cells using adenovirus-mediated decorin gene transfer. *FASEB J.* 2003;17(3):464-466.

14. Sulochana KN, Fan H, Jois S, Subramanian V, Sun F, Kini RM, Ge R. Peptides derived from human decorin leucine-rich repeat 5 inhibit angiogenesis. *J Biol Chem.* 2005;280(30):27935-27948.

15. Yamaguchi Y, Mann DM, Ruoslahti E. Negative regulation of transforming growth factor-beta by the proteoglycan decorin. *Nature.* 1990;346(6281):281-284.

16. Imai K, Hiramatsu A, Fukushima D, Pierschbacher MD, Okada Y. Degradation of decorin by matrix metalloproteinases: identification of the cleavage sites, kinetic analyses and transforming growth factor-beta1 release. *Biochem J.* 1997;322 (Pt 3):809-814.

17. Hildebrand A, Romaris M, Rasmussen LM, Heinegard D, Twardzik DR, Border WA, Ruoslahti E. Interaction of the small interstitial proteoglycans biglycan, decorin and fibromodulin with transforming growth factor beta. *Biochem J.* 1994;302 (Pt 2):527-534.

18. Fischer JW, Kinsella MG, Clowes MM, Lara S, Clowes AW, Wight TN. Local expression of bovine decorin by cell-mediated gene transfer reduces neointimal formation after balloon injury in rats. *Circ Res.* 2000;86(6):676-683.

19. Isaka Y, Brees DK, Ikegaya K, Kaneda Y, Imai E, Noble NA, Border WA. Gene therapy by skeletal muscle expression of decorin prevents fibrotic disease in rat kidney. *Nat Med.* 1996;2(4):418-423.

20. Giri SN, Hyde DM, Braun RK, Gaarde W, Harper JR, Pierschbacher MD. Antifibrotic effect of decorin in a bleomycin hamster model of lung fibrosis. *Biochem Pharmacol.* 1997;54(11):1205-1216.

21. Border WA, Noble NA, Yamamoto T, Harper JR, Yamaguchi Y, Pierschbacher MD, Ruoslahti E. Natural inhibitor of transforming growth factor-beta protects against scarring in experimental kidney disease. *Nature.* 1992;360(6402):361-364.

22. Weis SM, Zimmerman SD, Shah M, Covell JW, Omens JH, Ross J, Jr., Dalton N, Jones Y, Reed CC, Iozzo RV, McCulloch AD. A role for decorin in the remodeling of myocardial infarction. *Matrix Biol.* 2005;24(4):313-324.

23. Faust SM, Lu G, Wood SC, Bishop DK. TGFbeta neutralization within cardiac allografts by decorin gene transfer attenuates chronic rejection. *J Immunol.* 2009;183(11):7307-7313.

24. Yan W, Wang P, Zhao CX, Tang J, Xiao X, Wang DW. Decorin gene delivery inhibits cardiac fibrosis in spontaneously hypertensive rats by modulation of transforming growth factor-beta/Smad and p38 mitogen-activated protein kinase signaling pathways. *Hum Gene Ther.* 2009;20(10):1190-1200.

25. Davies JE, Tang X, Denning JW, Archibald SJ, Davies SJ. Decorin suppresses neurocan, brevican, phosphacan and NG2 expression and promotes axon growth across adult rat spinal cord injuries. *Eur J Neurosci.* 2004;19(5):1226-1242.

26. Grisanti S, Szurman P, Warga M, Kaczmarek R, Ziemssen F, Tatar O, Bartz-Schmidt KU. Decorin modulates wound healing in experimental glaucoma filtration surgery: a pilot study. *Invest Ophthalmol Vis Sci.* 2005;46(1):191-196.

27. Zhu J, Li Y, Shen W, Qiao C, Ambrosio F, Lavasani M, Nozaki M, Branca MF, Huard J. Relationships between transforming growth factor-beta1, myostatin,

and decorin: implications for skeletal muscle fibrosis. *J Biol Chem.* 2007;282(35):25852-25863.

28. Anderson JM. Inflammation, Wound Healing and the Foreign Body Response. In: Ratner BD, Hoffman, A. S., Schoen, F. J., Lemons, J. E., ed. *Biomaterials Scinece: An Introduction to Materials in Medicine*. 2nd ed. San Diego, CA: Elsevier Academic Press; 2004:296-304.

29. Anderson JM. Host Reactions to Biomaterials and Their Evaluation. In: Ratner BD, Hoffman, A. S., Schoen, F. J., Lemons, J. E., ed. *Biomaterials Science: An Introduction to Materials in Medicine*. 2nd ed. San Diego, CA: Elsevier Academic Press; 2004:165-214.

30. Ratner BD. Reducing capsular thickness and enhancing angiogenesis around implant drug release systems. *J Control Release.* 2002;78(1-3):211-218.

31. Sharkawy AA, Klitzman B, Truskey GA, Reichert WM. Engineering the tissue which encapsulates subcutaneous implants. II. Plasma-tissue exchange properties. *J Biomed Mater Res.* 1998;40(4):586-597.

32. Sharkawy AA, Klitzman B, Truskey GA, Reichert WM. Engineering the tissue which encapsulates subcutaneous implants. III. Effective tissue response times. *J Biomed Mater Res.* 1998;40(4):598-605.

33. Tang L, Eaton JW. Inflammatory responses to biomaterials. *Am J Clin Pathol.* 1995;103(4):466-471.

34. Ratner BD. New ideas in biomaterials science--a path to engineered biomaterials. *J Biomed Mater Res.* 1993;27(7):837-850.

35. Piscatelli SJ, Partington M, Hobar C, Gregory P, Siebert JW. Breast capsule contracture: is fibroblast activity associated with severity? *Aesthetic Plast Surg.* 1994;18(1):75-79.

36. Caffee HH. Textured silicone and capsule contracture. *Ann Plast Surg.* 1990;24(3):197-199.

37. Marques M, Brown SA, Oliveira I, Cordeiro MN, Morales-Helguera A, Rodrigues A, Amarante J. Long-term follow-up of breast capsule contracture rates in cosmetic and reconstructive cases. *Plast Reconstr Surg.*126(3):769-778.

38. Quaglini V, Mantero S, Villa T. Mechanical properties of breast periprosthetic capsules and the correlation to capsule contracture. *J Appl Biomater Biomech.* 2005;3(3):184-191.

39. Moreira M, Fagundes DJ, de Jesus Simoes M, Taha MO, Perez LM, Bazotte RB. The effect of liposome-delivered prednisolone on collagen density, myofibroblasts, and fibrous capsule thickness around silicone breast implants in rats. *Wound Repair Regen.*18(4):417-425.

40. Norton LW, Tegnell E, Toporek SS, Reichert WM. In vitro characterization of vascular endothelial growth factor and dexamethasone releasing hydrogels for implantable probe coatings. *Biomaterials.* 2005;26(16):3285-3297.

41. Gerritsen M, Kros A, Sprakel V, Lutterman JA, Nolte RJ, Jansen JA. Biocompatibility evaluation of sol-gel coatings for subcutaneously implantable glucose sensors. *Biomaterials.* 2000;21(1):71-78.

42. Gombotz WR, Wang GH, Horbett TA, Hoffman AS. Protein adsorption to poly(ethylene oxide) surfaces. *J Biomed Mater Res.* 1991;25(12):1547-1562.

43. Cao L, Sukavaneshvar S, Ratner BD, Horbett TA. Glow discharge plasma treatment of polyethylene tubing with tetraglyme results in ultralow fibrinogen adsorption and greatly reduced platelet adhesion. *J Biomed Mater Res A.* 2006;79(4):788-803.

44. Cao L, Chang M, Lee CY, Castner DG, Sukavaneshvar S, Ratner BD, Horbett TA. Plasma-deposited tetraglyme surfaces greatly reduce total blood protein adsorption, contact activation, platelet adhesion, platelet procoagulant activity, and in vitro thrombus deposition. *J Biomed Mater Res A.* 2007;81(4):827-837.

45. Hetrick EM, Prichard HL, Klitzman B, Schoenfisch MH. Reduced foreign body response at nitric oxide-releasing subcutaneous implants. *Biomaterials.* 2007;28(31):4571-4580.

46. Ward WK, Quinn MJ, Wood MD, Tiekotter KL, Pidikiti S, Gallagher JA. Vascularizing the tissue surrounding a model biosensor: how localized is the effect of a subcutaneous infusion of vascular endothelial growth factor (VEGF)? *Biosens Bioelectron.* 2003;19(3):155-163.

47. Ravin AG, Olbrich KC, Levin LS, Usala AL, Klitzman B. Long- and short-term effects of biological hydrogels on capsule microvascular density around implants in rats. *J Biomed Mater Res.* 2001;58(3):313-318.

48. Norton LW, Koschwanez HE, Wisniewski NA, Klitzman B, Reichert WM. Vascular endothelial growth factor and dexamethasone release from nonfouling sensor coatings affect the foreign body response. *J Biomed Mater Res A.* 2007;81(4):858-869.

49. Ward WK, Slobodzian EP, Tiekotter KL, Wood MD. The effect of microgeometry, implant thickness and polyurethane chemistry on the foreign body response to subcutaneous implants. *Biomaterials.* 2002;23(21):4185-4192.

50. Marshall AJ. *Porous Hydrogels with Well-Defined Pore Structure for Biomaterials Applications*. Seattle: Department of Bioengineering, University of Washington; 2004.

51. Osathanon T, Linnes ML, Rajachar RM, Ratner BD, Somerman MJ, Giachelli CM. Microporous nanofibrous fibrin-based scaffolds for bone tissue engineering. *Biomaterials.* 2008;29(30):4091-4099.

52. Linnes MP, Ratner BD, Giachelli CM. A fibrinogen-based precision microporous scaffold for tissue engineering. *Biomaterials.* 2007;28(35):5298-5306.

53. Madden LR, Mortisen DJ, Sussman EM, Dupras SK, Fugate JA, Cuy JL, Hauch KD, Laflamme MA, Murry CE, Ratner BD. Proangiogenic scaffolds as functional templates for cardiac tissue engineering. *Proc Natl Acad Sci U S A.*107(34):15211-15216.

54. Sanders JE, Rochefort JR. Fibrous encapsulation of single polymer microfibers depends on their vertical dimension in subcutaneous tissue. *J Biomed Mater Res A.* 2003;67(4):1181-1187.

55. Sanders JE, Stiles CE, Hayes CL. Tissue response to single-polymer fibers of varying diameters: evaluation of fibrous encapsulation and macrophage density. *J Biomed Mater Res.* 2000;52(1):231-237.

56. Zeplin PH, Larena-Avellaneda A, Jordan M, Laske M, Schmidt K. Phosphorylcholine-coated silicone implants: effect on inflammatory response and fibrous capsule formation. *Ann Plast Surg.*65(6):560-564.

57. Abramo AC, De Oliveira VR, Ledo-Silva MC, De Oliveira EL. How texture-inducing contraction vectors affect the fibrous capsule shrinkage around breasts implants? *Aesthetic Plast Surg.*34(5):555-560.

58. Suska F, Emanuelsson L, Johansson A, Tengvall P, Thomsen P. Fibrous capsule formation around titanium and copper. *J Biomed Mater Res A.* 2008;85(4):888-896.

59. Takahashi H, Wang Y, Grainger DW. Device-based local delivery of siRNA against mammalian target of rapamycin (mTOR) in a murine subcutaneous implant model to inhibit fibrous encapsulation. *J Control Release.*147(3):400-407.

60. Kyriakides TR, Leach KJ, Hoffman AS, Ratner BD, Bornstein P. Mice that lack the angiogenesis inhibitor, thrombospondin 2, mount an altered foreign body reaction characterized by increased vascularity. *Proc Natl Acad Sci U S A.* 1999;96(8):4449-4454.

61. Kyriakides TR, Foster MJ, Keeney GE, Tsai A, Giachelli CM, Clark-Lewis I, Rollins BJ, Bornstein P. The CC chemokine ligand, CCL2/MCP1, participates in macrophage fusion and foreign body giant cell formation. *Am J Pathol.* 2004;165(6):2157-2166.

62. Jarvelainen H, Puolakkainen P, Pakkanen S, Brown EL, Hook M, Iozzo RV, Sage EH, Wight TN. A role for decorin in cutaneous wound healing and angiogenesis. *Wound Repair Regen.* 2006;14(4):443-452.

63. O'Kane S, Ferguson MW. Transforming growth factor beta s and wound healing. *Int J Biochem Cell Biol.* 1997;29(1):63-78.

64. Leask A, Abraham DJ. TGF-beta signaling and the fibrotic response. *FASEB J.* 2004;18(7):816-827.

65. Sporn MB, Roberts AB. The transforming growth factor-betas: past, present, and future. *Ann N Y Acad Sci.* 1990;593:1-6.

66. Massague J. The transforming growth factor-beta family. *Annu Rev Cell Biol.* 1990;6:597-641.

67. Miyazono K, Ichijo H, Heldin CH. Transforming growth factor-beta: latent forms, binding proteins and receptors. *Growth Factors.* 1993;8(1):11-22.

68. Derynck R, Feng XH. TGF-beta receptor signaling. *Biochim Biophys Acta.* 1997;1333(2):F105-150.

69. Bernasconi P, Torchiana E, Confalonieri P, Brugnoni R, Barresi R, Mora M, Cornelio F, Morandi L, Mantegazza R. Expression of transforming growth factor-beta 1 in dystrophic patient muscles correlates with fibrosis. Pathogenetic role of a fibrogenic cytokine. *J Clin Invest.* 1995;96(2):1137-1144.

70. Tiggelman AM, Linthorst C, Boers W, Brand HS, Chamuleau RA. Transforming growth factor-beta-induced collagen synthesis by human liver myofibroblasts is inhibited by alpha2-macroglobulin. *J Hepatol.* 1997;26(6):1220-1228.

71. Yokozeki M, Moriyama K, Shimokawa H, Kuroda T. Transforming growth factor-beta 1 modulates myofibroblastic phenotype of rat palatal fibroblasts in vitro. *Exp Cell Res.* 1997;231(2):328-336.

72. Kane CJ, Hebda PA, Mansbridge JN, Hanawalt PC. Direct evidence for spatial and temporal regulation of transforming growth factor beta 1 expression during cutaneous wound healing. *J Cell Physiol.* 1991;148(1):157-173.

73. LeRoy EC, Trojanowska MI, Smith EA. Cytokines and human fibrosis. *Eur Cytokine Netw.* 1990;1(4):215-219.

74. Lin RY, Sullivan KM, Argenta PA, Meuli M, Lorenz HP, Adzick NS. Exogenous transforming growth factor-beta amplifies its own expression and induces scar formation in a model of human fetal skin repair. *Ann Surg.* 1995;222(2):146-154.

75. Sullivan KM, Lorenz HP, Meuli M, Lin RY, Adzick NS. A model of scarless human fetal wound repair is deficient in transforming growth factor beta. *J Pediatr Surg.* 1995;30(2):198-202; discussion 202-193.

76. Duncan MR, Frazier KS, Abramson S, Williams S, Klapper H, Huang X, Grotendorst GR. Connective tissue growth factor mediates transforming growth factor beta-induced collagen synthesis: down-regulation by cAMP. *FASEB J.* 1999;13(13):1774-1786.

77. Chen K, Wei Y, Sharp GC, Braley-Mullen H. Inhibition of TGFbeta1 by anti-TGFbeta1 antibody or lisinopril reduces thyroid fibrosis in granulomatous experimental autoimmune thyroiditis. *J Immunol.* 2002;169(11):6530-6538.

78. Schultze-Mosgau S, Wehrhan F, Rodel F, Amann K, Radespiel-Troger M, Kopp J, Grabenbauer G. Anti-TGFbeta1 antibody for modulation of expression of endogenous transforming growth factor beta 1 to prevent fibrosis after plastic surgery in rats. *Br J Oral Maxillofac Surg.* 2004;42(2):112-119.

79. Rosenberg LC, Choi HU, Tang LH, Johnson TL, Pal S, Webber C, Reiner A, Poole AR. Isolation of dermatan sulfate proteoglycans from mature bovine articular cartilages. *J Biol Chem.* 1985;260(10):6304-6313.

80. Damle SP, Coster L, Gregory JD. Proteodermatan sulfate isolated from pig skin. *J Biol Chem.* 1982;257(10):5523-5527.

81. Heinegard D, Paulsson M, Inerot S, Carlstrom C. A novel low-molecular weight chondroitin sulphate proteoglycan isolated from cartilage. *Biochem J.* 1981;197(2):355-366.

82. Krusius T, Ruoslahti E. Primary structure of an extracellular matrix proteoglycan core protein deduced from cloned cDNA. *Proc Natl Acad Sci U S A.* 1986;83(20):7683-7687.

83. Kresse H, Hausser H, Schonherr E, Bittner K. Biosynthesis and interactions of small chondroitin/dermatan sulphate proteoglycans. *Eur J Clin Chem Clin Biochem.* 1994;32(4):259-264.

84. Keene DR, San Antonio JD, Mayne R, McQuillan DJ, Sarris G, Santoro SA, Iozzo RV. Decorin binds near the C terminus of type I collagen. *J Biol Chem.* 2000;275(29):21801-21804.

85. Hedbom E, Heinegard D. Binding of fibromodulin and decorin to separate sites on fibrillar collagens. *J Biol Chem.* 1993;268(36):27307-27312.

86. Svensson L, Heinegard D, Oldberg A. Decorin-binding sites for collagen type I are mainly located in leucine-rich repeats 4-5. *J Biol Chem.* 1995;270(35):20712-20716.

87. Kalamajski S, Aspberg A, Oldberg A. The decorin sequence SYIRIADTNIT binds collagen type I. *J Biol Chem.* 2007;282(22):16062-16067.

88. Grant DS, Yenisey C, Rose RW, Tootell M, Santra M, Iozzo RV. Decorin suppresses tumor cell-mediated angiogenesis. *Oncogene.* 2002;21(31):4765-4777.

89. Davies Cde L, Melder RJ, Munn LL, Mouta-Carreira C, Jain RK, Boucher Y. Decorin inhibits endothelial migration and tube-like structure formation: role of thrombospondin-1. *Microvasc Res.* 2001;62(1):26-42.

90. Tran KT, Griffith L, Wells A. Extracellular matrix signaling through growth factor receptors during wound healing. *Wound Repair Regen.* 2004;12(3):262-268.

91. Mohan RR, Tovey JC, Sharma A, Schultz GS, Cowden JW, Tandon A. Targeted decorin gene therapy delivered with adeno-associated virus effectively retards corneal neovascularization in vivo. *PLoS One.*6(10):e26432.

92. Mohan RR, Tandon A, Sharma A, Cowden JW, Tovey JC. Significant inhibition of corneal scarring in vivo with tissue-selective, targeted AAV5 decorin gene therapy. *Invest Ophthalmol Vis Sci.*52(7):4833-4841.

93. Takeuchi Y, Kodama Y, Matsumoto T. Bone matrix decorin binds transforming growth factor-beta and enhances its bioactivity. *J Biol Chem.* 1994;269(51):32634-32638.

94. Schonherr E, Broszat M, Brandan E, Bruckner P, Kresse H. Decorin core protein fragment Leu155-Val260 interacts with TGF-beta but does not compete for decorin binding to type I collagen. *Arch Biochem Biophys.* 1998;355(2):241-248.

95. Kresse H, Liszio C, Schonherr E, Fisher LW. Critical role of glutamate in a central leucine-rich repeat of decorin for interaction with type I collagen. *J Biol Chem.* 1997;272(29):18404-18410.

96. Fukushima K, Badlani N, Usas A, Riano F, Fu F, Huard J. The use of an antifibrosis agent to improve muscle recovery after laceration. *Am J Sports Med.* 2001;29(4):394-402.

97. Border WA, Okuda S, Languino LR, Sporn MB, Ruoslahti E. Suppression of experimental glomerulonephritis by antiserum against transforming growth factor beta 1. *Nature.* 1990;346(6282):371-374.

98. Nili N, Cheema AN, Giordano FJ, Barolet AW, Babaei S, Hickey R, Eskandarian MR, Smeets M, Butany J, Pasterkamp G, Strauss BH. Decorin inhibition of PDGF-stimulated vascular smooth muscle cell function: potential

mechanism for inhibition of intimal hyperplasia after balloon angioplasty. *Am J Pathol.* 2003;163(3):869-878.

99. Sato K, Li Y, Foster W, Fukushima K, Badlani N, Adachi N, Usas A, Fu FH, Huard J. Improvement of muscle healing through enhancement of muscle regeneration and prevention of fibrosis. *Muscle Nerve.* 2003;28(3):365-372.

100. Fischer JW, Kinsella MG, Levkau B, Clowes AW, Wight TN. Retroviral overexpression of decorin differentially affects the response of arterial smooth muscle cells to growth factors. *Arterioscler Thromb Vasc Biol.* 2001;21(5):777-784.

101. Martin SM, Schwartz JL, Giachelli CM, Ratner BD. Enhancing the biological activity of immobilized osteopontin using a type-1 collagen affinity coating. *J Biomed Mater Res A.* 2004;70(1):10-19.

102. Di Lullo GA, Sweeney SM, Korkko J, Ala-Kokko L, San Antonio JD. Mapping the ligand-binding sites and disease-associated mutations on the most abundant protein in the human, type I collagen. *J Biol Chem.* 2002;277(6):4223-4231.

103. Zwadlo-Klarwasser G, Gorlitz K, Hafemann B, Klee D, Klosterhalfen B. The chorioallantoic membrane of the chick embryo as a simple model for the study of the angiogenic and inflammatory response to biomaterials. *J Mater Sci Mater Med.* 2001;12(3):195-199.

104. Lange N, Ballini JP, Wagnieres G, van den Bergh H. A new drug-screening procedure for photosensitizing agents used in photodynamic therapy for CNV. *Invest Ophthalmol Vis Sci.* 2001;42(1):38-46.

105. Valdes TI, Kreutzer D, Moussy F. The chick chorioallantoic membrane as a novel in vivo model for the testing of biomaterials. *J Biomed Mater Res.* 2002;62(2):273-282.

106. Leibovich SJ, Polverini PJ, Shepard HM, Wiseman DM, Shively V, Nuseir N. Macrophage-induced angiogenesis is mediated by tumour necrosis factor-alpha. *Nature.* 1987;329(6140):630-632.

107. Klueh U, Dorsky DI, Moussy F, Kreutzer DL. Ex ova chick chorioallantoic membrane as a novel model for evaluation of tissue responses to biomaterials and implants. *J Biomed Mater Res A.* 2003;67(3):838-843.

108. Valdes TI, Klueh U, Kreutzer D, Moussy F. Ex ova chick chorioallantoic membrane as a novel in vivo model for testing biosensors. *J Biomed Mater Res A.* 2003;67(1):215-223.

109. Lhoest JB, Wagner MS, Tidwell CD, Castner DG. Characterization of adsorbed protein films by time of flight secondary ion mass spectrometry. *J Biomed Mater Res.* 2001;57(3):432-440.

110. Wagner MS, Tyler BJ, Castner DG. Interpretation of static time-of-flight secondary ion mass spectra of adsorbed protein films by multivariate pattern recognition. *Anal Chem.* 2002;74(8):1824-1835.

111. Karp FB, Bernotski NA, Valdes TI, Bohringer KF, Ratner BD. Foreign Body Response Investigated With an Implanted Biosensor by *In Situ* Electrical Impedance Spectroscopy. *IEEE Sensors Journal.* 2008;8(1):104-112.

112. Bhide VM, Laschinger CA, Arora PD, Lee W, Hakkinen L, Larjava H, Sodek J, McCulloch CA. Collagen phagocytosis by fibroblasts is regulated by decorin. *J Biol Chem.* 2005;280(24):23103-23113.

113. Kidd KR, Dal Ponte DB, Kellar RS, Williams SK. A comparative evaluation of the tissue responses associated with polymeric implants in the rat and mouse. *J Biomed Mater Res.* 2002;59(4):682-689.

114. Clowes MM, Lynch CM, Miller AD, Miller DG, Osborne WR, Clowes AW. Long-term biological response of injured rat carotid artery seeded with smooth muscle cells expressing retrovirally introduced human genes. *J Clin Invest.* 1994;93(2):644-651.

115. Miller AD, Rosman GJ. Improved retroviral vectors for gene transfer and expression. *Biotechniques.* 1989;7(9):980-982, 984-986, 989-990.

116. Kinsella MG, Fischer JW, Mason DP, Wight TN. Retrovirally mediated expression of decorin by macrovascular endothelial cells. Effects on cellular migration and fibronectin fibrillogenesis in vitro. *J Biol Chem.* 2000;275(18):13924-13932.

117. Fisher LW, Stubbs JT, 3rd, Young MF. Antisera and cDNA probes to human and certain animal model bone matrix noncollagenous proteins. *Acta Orthop Scand Suppl.* 1995;266:61-65.

118. Junqueira LC, Bignolas G, Brentani RR. Picrosirius staining plus polarization microscopy, a specific method for collagen detection in tissue sections. *Histochem J.* 1979;11(4):447-455.

119. Ulger H, Karabulut AK, Pratten MK. Labelling of rat endothelial cells with antibodies to vWF, RECA-1, PECAM-1, ICAM-1, OX-43 and ZO-1. *Anat Histol Embryol.* 2002;31(1):31-35.

120. Hausser H, Groning A, Hasilik A, Schonherr E, Kresse H. Selective inactivity of TGF-beta/decorin complexes. *FEBS Lett.* 1994;353(3):243-245.

121. Jarvinen TA, Ruoslahti E. Target-seeking antifibrotic compound enhances wound healing and suppresses scar formation in mice. *Proc Natl Acad Sci U S A.*107(50):21671-21676.

122. Ismail JA, Poppa V, Kemper LE, Scatena M, Giachelli CM, Coffin JD, Murry CE. Immunohistologic labeling of murine endothelium. *Cardiovasc Pathol.* 2003;12(2):82-90.

123. Toma C, Wagner WR, Bowry S, Schwartz A, Villanueva F. Fate of culture-expanded mesenchymal stem cells in the microvasculature: in vivo observations of cell kinetics. *Circ Res.* 2009;104(3):398-402.

124. Yang PC. Is Reliable in vivo Detection of Stem Cell Viability Possible in a Large Animal Model of Myocardial Injury? *Circulation.*

125. Jalili RB, Moeen Rezakhanlou A, Hosseini-Tabatabaei A, Ao Z, Warnock GL, Ghahary A. Fibroblast populated collagen matrix promotes islet survival and reduces the number of islets required for diabetes reversal. *J Cell Physiol.*226(7):1813-1819.

126. Cheng JY, Raghunath M, Whitelock J, Poole-Warren L. Matrix components and scaffolds for sustained islet function. *Tissue Eng Part B Rev.*17(4):235-247.

127. Neill T, Painter H, Buraschi S, Owens RT, Lisanti MP, Schaefer L, Iozzo RV. Decorin antagonizes the angiogenic network: concurrent inhibition of Met, hypoxia inducible factor 1alpha, vascular endothelial growth factor A, and induction of thrombospondin-1 and TIMP3. *J Biol Chem.*287(8):5492-5506.

128. Buraschi S, Pal N, Tyler-Rubinstein N, Owens RT, Neill T, Iozzo RV. Decorin antagonizes Met receptor activity and down-regulates {beta}-catenin and Myc levels. *J Biol Chem.*285(53):42075-42085.

129. Theocharis AD, Skandalis SS, Tzanakakis GN, Karamanos NK. Proteoglycans in health and disease: novel roles for proteoglycans in malignancy and their pharmacological targeting. *FEBS J.*277(19):3904-3923.

130. Hu Y, Sun H, Owens RT, Wu J, Chen YQ, Berquin IM, Perry D, O'Flaherty JT, Edwards IJ. Decorin suppresses prostate tumor growth through inhibition of epidermal growth factor and androgen receptor pathways. *Neoplasia.* 2009;11(10):1042-1053.

131. Araki K, Wakabayashi H, Shintani K, Morikawa J, Matsumine A, Kusuzaki K, Sudo A, Uchida A. Decorin suppresses bone metastasis in a breast cancer cell line. *Oncology.* 2009;77(2):92-99.

132. Goldoni S, Iozzo RV. Tumor microenvironment: Modulation by decorin and related molecules harboring leucine-rich tandem motifs. *Int J Cancer.* 2008;123(11):2473-2479.

133. Goldoni S, Seidler DG, Heath J, Fassan M, Baffa R, Thakur ML, Owens RT, McQuillan DJ, Iozzo RV. An antimetastatic role for decorin in breast cancer. *Am J Pathol.* 2008;173(3):844-855.

134. Stuart K, Paderi J, Snyder PW, Freeman L, Panitch A. Collagen-binding peptidoglycans inhibit MMP mediated collagen degradation and reduce dermal scarring. *PLoS One.*6(7):e22139.

VITA

Marisa Sylvester was born in Baton Rouge, Louisiana, to Allen and Wannipa
Sylvester. She graduated with honors from Baton Rouge Magnet High School in 1999.
She completed pre-medicine requirements at Louisiana State University and graduated
summa cum laude with a Bachelor of Science in Biological Engineering in 2003. She
conducted research in the lab of Dr. Kelly A. Rusch in the Environmental Engineering
Department at LSU. She then moved to Seattle, Washington, to pursue a PhD at the
University of Washington. She completed her graduate research in the lab of Dr.
Buddy D. Ratner and earned a Doctor of Philosophy from the Department of
Bioengineering in 2012.